8-2009

High-sensitivity spectral fluorescence lifetime imaging for resolving spectroscopically overlapping species

Justin Lee Crawford
University of Tennessee Space Institute, jcrawf25@utk.edu

To the Graduate Council:

I am submitting herewith a thesis written by Justin Lee Crawford entitled "High-sensitivity spectral fluorescence lifetime imaging for resolving spectroscopically overlapping species." I have examined the final electronic copy of this thesis for form and content and recommend that it be accepted in partial fulfillment of the requirements for the degree of Master of Science, with a major in Physics and Astronomy.

Lloyd M. Davis, Major Professor

We have read this thesis and recommend its acceptance:

Horace W. Crater, Christian G. Parigger

Accepted for the Council:
Carolyn R. Hodges

Vice Provost and Dean of the Graduate School

(Original signatures are on file with official student records.)

To the Graduate Council:

I am submitting herewith a thesis written by Justin L. Crawford entitled “High-sensitivity spectral fluorescence lifetime imaging for resolving spectroscopically overlapping species.” I have examined the final electronic copy of this thesis for form and content and recommend that it be accepted in partial fulfillment of the requirements for the degree of Master of Science, with a major in Physics.

Lloyd M. Davis, Major Professor

We have read this thesis
and recommend its acceptance:

Lloyd M. Davis

Horace W. Crater

Christian G. Parigger

Accepted for the Council:

Carolyn R. Hodges
Vice Provost and Dean of the Graduate School

High-sensitivity spectral fluorescence lifetime imaging for resolving spectroscopically overlapping species

A Thesis Presented for
The Master of Science
Degree
The University of Tennessee, Knoxville

Justin L. Crawford
August 2009

Acknowledgements

This research was funded in part by the National Institute of Health under the grant 1R03EB004586-01A1. Thank you to Dr. Lloyd M. Davis for his much appreciated guidance and teaching. On a personal note, I would like to thank all those who have stood by me over the years, especially my parents.

Abstract

The capability to resolve the contributions from spectroscopically overlapping fluorophores has enabled significant breakthroughs in cellular imaging. However, commercial microscopes for this purpose use analog light detection with least squares curve-fitting analysis and improvements in sensitivity are needed. To this end, a microscope has been constructed with high throughput and single-photon detection capability. The fluorescence is separated through use of a prism spectrometer or a series of dichroic mirrors into four spectral bands and detected using four single-photon avalanche diode (SPAD) detectors, which provide high-quantum efficiency in the red spectral region. The detectors are connected to a time-correlated single photon counting module to provide sub-nanosecond temporal resolution for distinguishing fluorophores with different fluorescence lifetimes. Maximum-likelihood (ML) methods have been developed for analyzing the temporally and spectrally resolved photon count data from the SPADs to find the contributions from different fluorescent species and from background. Commercially available SPADs exhibit a count-rate dependent time shift in the impulse response function, and hence the instrument incorporates custom modified SPADs with improved timing stability. Nevertheless, there is still some time shift, and hence the ML-analysis has been extended to include this as an adjustable parameter for each individual SPAD. Monte Carlo simulations have also been developed to enable studies of the number of photons needed to resolve specific fluorophores.

Table of contents

List of figures

Chapter I

Introduction

Multi-dimensional imaging, in which spectroscopic information is collected at each pixel of an image, is a developing tool that has already enabled breakthrough results in biophysical research [1]. This thesis presents research on improving the sensitivity of temporally and spectrally resolved imaging for applications that require resolution of signal contributions from fluorescent species with overlapping spectra. One specific area in which this is important is when imaging intrinsically fluorescent proteins (IFPs). These are now widely used as noninvasive site-specific markers in cellular biophysics experiments. In order to get more information from experiments, many applications require the imaging of multiple IFPs. However, in high-sensitivity cellular imaging, clear separation of the variants of IFPs and auto-fluorescence remains a challenge.

In order to achieve the goal of multi-dimensional imaging with high sensitivity, new instrumentation and data analysis methods must be developed. To this end, the first key undertaking of this thesis is the setup of a confocal microscope with single-molecule detection sensitivity. It employs a high throughput spectrometer and four single-photon avalanche diode (SPAD) detectors, which give high quantum efficiency in the red region of the spectrum and which have been modified to provide stable sub-nanosecond timing. The second key undertaking is the development of maximum-likelihood

techniques for resolving (i.e., linearly unmixing) the signal contributions from different species in the sample in experiments where there are low numbers of photons in a spectroscopic channel.

In this thesis, Chapter 2 presents a brief background of the techniques and equipment. In Chapter 3, a more in-depth account is given on how linear unmixing is accomplished and why specific methods were used. In Chapter 4, the setup of the experiment is brought into focus to give insight into important aspects and issues to avoid. Also in Chapter 4, data acquisition will be examined, with emphasis on file types and how to process their embedded information. With these initial steps of the experiment laid out, results are discussed in Chapter 5 as well as their meaning and importance. Finally, concluding remarks are given in Chapter 6 along with suggestions for where the experiments could progress in the future.

Chapter II

Background

As stated in the introduction, fluorescence spectroscopy has become an essential tool in cellular and molecular imaging for biological and biophysical research. As interest increases about the inner working of cellular processes, the development and application of fluorescent protein markers has also risen [2,3]. Their application includes the possibility to view several cellular processes at once, each specified with its own marker. Although this idea promises great bounds for detailed information, it is hindered by the issue of crosstalk. The emission spectra of most fluorophores are shaped with a steep increase towards the peak, corresponding to the onset at shorter wavelengths, followed by a long emission tail [4]. When fluorophores have spectra in similar wavelength regions, this tail generally overlaps with the spectra of other fluorophores and leads to crosstalk. This crosstalk makes multispectral imaging difficult as it is nearly impossibly to see which signal comes from which fluorophore without further data processing. In order to deal with this issue, the idea of linear unmixing arose, allowing researchers to measure and calibrate the crosstalk and then mathematically estimate the signal contributions from each of the fluorophores in the sample.

In this chapter, commercial systems are reviewed to give insight on the current state of technology. The purpose of this research is then restated, with an emphasis on how to improve what is currently available. From there, background information on the individual parts of the experiment is presented, together with explanation of why each is chosen. These topics include SPADs, confocal microscopy, time-correlated single photon counting (TCSPC) modules, prism spectroscopy and interference filters, and maximum-likelihood estimation (MLE).

2.1 Commercial instrumentation

The main microscope systems currently available for fluorescence spectroscopy when there are fluorophores with overlapping spectra are the Zeiss META [5] and the Leica TCS series [6]. These systems have become very popular in the field, especially in the study of Förster resonance energy transfer (FRET) [7]. Due to their ease of use and integrated software, users can digitally set parameters for their experiments as the systems adjust wavelengths, take images, and analyze and plot data. The Zeiss META takes advantage of nondescanned detectors to "fingerprint", the excitation spectra. This means that data from known samples are scanned and stored (as spectral fingerprints) to be compared later to unknown experimental samples. By applying this and the "excitation lambda stacks" created in the experiment, Dickinson *et al.* were able to remove autofluorescence and create crosstalk-free images for dyes with closely overlapping emission spectra [8]. Excitation lambda stacks are generated by taking a

large number of images while varying the excitation wavelength. Nondescanned detection means that the beam of collected fluorescence does *not* return through the mirrors that raster scan the excitation beam, and this causes it to scan over a small area across the face of the detector. Hence detectors such as photomultipliers with a sufficiently large surface area must be used, rather than high quantum efficiency SPAD detectors, which have very small active areas.

2.2 Current goals

The systems described in Section 2.1, though very useful and implemented in numerous experimental setups, have their limitations and drawbacks. One of these is that they cannot successfully resolve a mixture of fluorophores for low photon counts. As the counts get fewer and fewer, to the range of only 100 or less in any spectral channel, these systems fail (see discussion in Section 3.2). The first goal of this thesis is to determine how to take the concept of linear unmixing and apply it with ML analysis to cases when few counts are collected in any single spectral channel.

The second goal is to incorporate the capability for resolving spectrally similar fluorophores by also collecting fluorescence lifetime data, to enable unmixing of components with different fluorescence lifetimes. This is achieved by applying pulsed laser excitation and time-resolved photon detection. The concept of using temporal resolution is used in fluorescence lifetime imaging microscopy (FLIM), and this has been

combined with resolution of the emission spectrum (spectral FLIM or SLIM). Becker *et al.* have explored this multispectral FLIM idea in a 2007 paper [9].

Because of the potential sensitivity involved with fluorescence detection, it is desirable to collect the maximum amount of photons, with as little going to waste as possible. The general idea and discussion of importance can be found in reference [1]. Thus the third goal of this work is to build a microscope with high collection efficiency of fluorescence, with high optical throughput, and which incorporates SPAD detectors with high quantum efficiency (QE).

2.3 Single-photon avalanche diode detectors

SPAD detectors were created to measure single photons in experiments, but with better efficiency than photomultipliers. Avalanche photodiodes (APDs) typically have a large active area and are prone to thermally generated dark counts and hence they are suitable for use in applications where the light level is considerably higher. Microchannel plate photomultipliers (MCP-PMT), another possibility, are able to detect single photons, but have a rather low quantum efficiency of only 5–8%. Because of these reasons, they were not considered for this experiment. A brief description of what a SPAD is can be found in reference [10]:

> "The SPAD is essentially a *p-n* junction reverse biased above the breakdown voltage such that the junction electric field is sufficiently high to sustain the flow of an avalanche current triggered by a photogenerated carrier."

Presently, single photon counting modules (SPCMs) containing a SPAD are commercially available from several vendors, but only the SPCM from Perkin Elmer provides high quantum efficiency (~65%) at the red wavelengths typically used in fluorescence microscopy. Unfortunately, the electronics within this module suffer from a count-rate dependent time-walk due to a slow pick-up in the active quenching circuit (AQC). The function of the AQC is "to sense the rise of the avalanche pulse and react back on the SPAD, forcing, with a controlled bias-voltage source, the quenching and reset transitions in short times" [11]. The count-rate dependent time walk can be seen in Figure 1 and the effects of this time shift on an attempt to unmix a temporal spectrum can be seen in Figure 2. The optimized linear combination of fingerprint spectra does not match the spectral data from the mixture, as seen in the plot of the residues, because the average photon count rate during collection of the spectrum from the mixture differs from those of the fingerprint spectra.

In order to remove this effect from the detectors, a modification is necessary. Micro Photon Devices (MPD), a company based in Italy and established by Professor Sergio

Cova at the Poytechnico di Milano, produces SPAD photon counting modules with stable timing, albeit with lower quantum efficiency. Their modules incorporate the patented active quenching circuit shown in Figure 3, which alleviates the time-walk issue. In short, a pick-up capacitor is placed in the circuitry to allow for a faster output pulse. The Perkin Elmer SPCM modules were sent to MPD so that the high-QE SPADs from these modules could be incorporated into an active quenching circuit made by MPD. The timing jitter results measured by MPD are seen in Figure 4 [12].

As seen in Figure 3, the pick-up capacitor leads to a NIM pulse output, although a TTL pulse is also available. By comparison, the Perkin Elmer SPCM modules only provide a TTL pulse output. In order to achieve the fastest possible timing in the experiment, the NIM output must be used. Unfortunately, the Picoquant TimeHarp 200 available in our lab for TCSPC only accepts TTL pulses, and when the Perkin Elmer SPAD with MPD AQC is used with TTL output pulses, a count-rate dependent time walk is still present. To address this issue, efforts are being made to replace the Time Harp 200 with the Picoquant HydraHarp, which is a later model unit for TCSPC, or to add a circuit to convert the NIM pulses to TTL pulses. In this thesis research, the remaining count-rate dependant time-walk is addressed by including an adjustable time-shift in the fingerprint spectra when analyzing the spectra of mixtures, as discussed in Section 3.3.

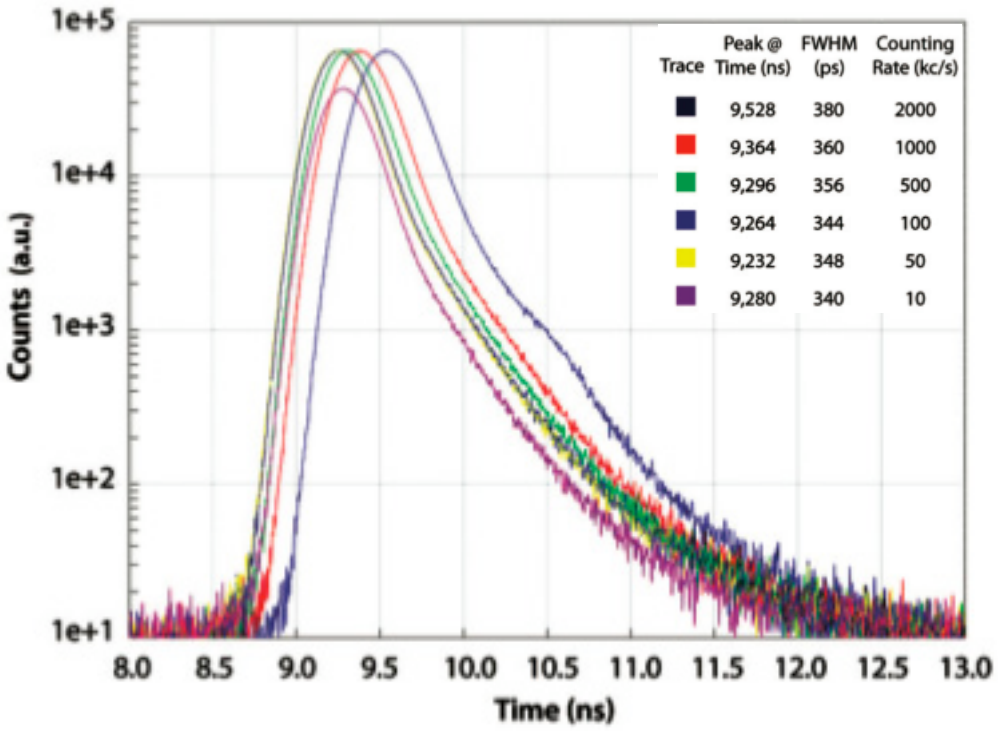

Figure 1: Measured timing jitter from unmodified Perkin-Elmer SPCM-AQR-14 exhibiting a time shift to later times with increasing mean count rate [12]

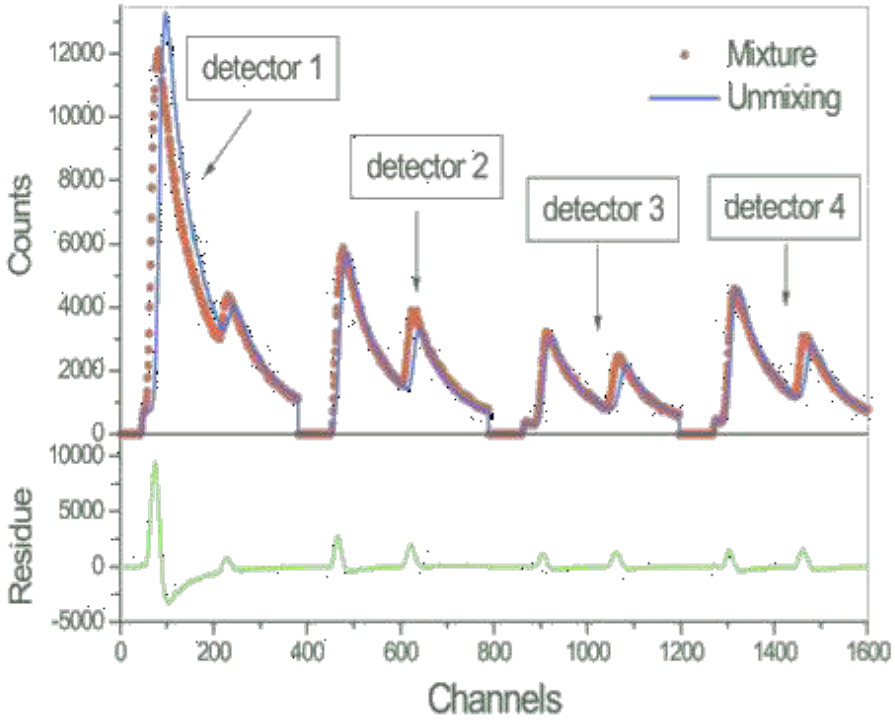

Figure 2: Mixture vs fit from unmixing. The time walk can be seen in the offset from the fit and data curve. It is more distinct when looking at the residue.

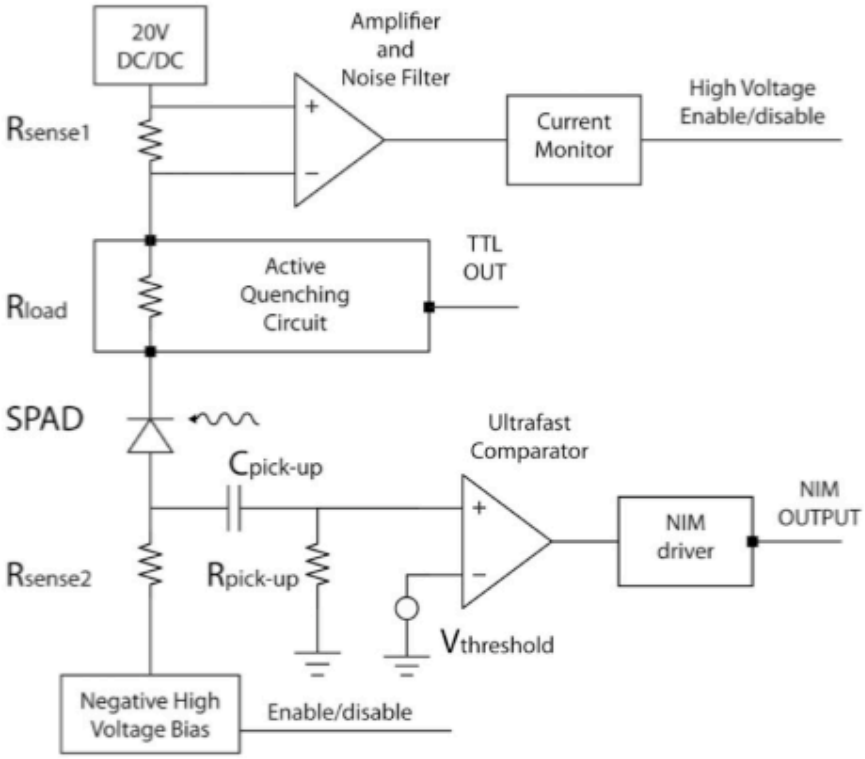

Figure 3: Schematic of modified SPAD detector [12]

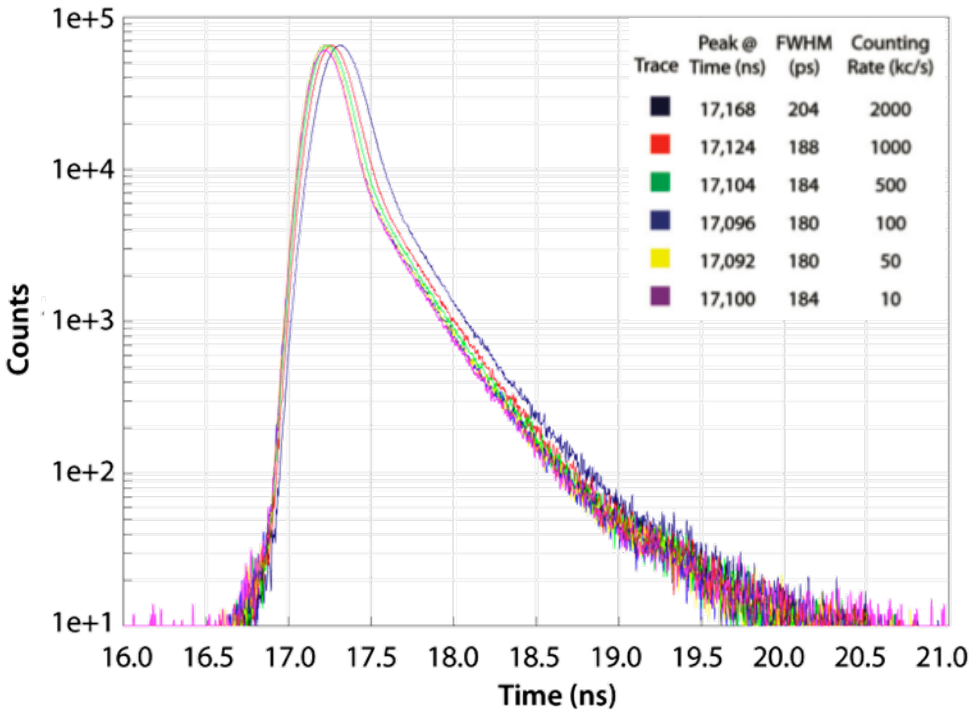

Figure 4: Time jitter measured in modified SPAD detector [12]

2.4 Confocal microscopy

As the experiment calls for use of a small sample volume and, more importantly, the use of only photons generated by the fluorescence of the sample, confocal microscopy is the most suitable technique available. An example of a confocal setup can be seen in Figure 5. A pinhole placed within the microscope, after the dichroic mirror and tube lens, makes it possible to eliminate out-of-focus light from the detector. This decreases any chance for stray light to enter into the system and skew the quality of the acquired data. As shown in Figure 5, in order for photons to reach the SPAD, they must originate from the confocal plane to be focused by the objective and tube lens through the pinhole. Any rays that are focused elsewhere will be rejected by the system as their paths are skewed away from the pinhole.

For imaging, acquisition rates are limited by scanning speeds. A good review of the different systems and their advantages/disadvantages can be found in reference [13]. Along with an introduction to different techniques, the reference also advises on certain aspects to keep in mind to achieve better results when doing experiments. These include, among others, the use of as few optical elements as possible, removing unwanted wavelengths with filters, and the use of high numerical aperture objectives to provide the greatest possible collection of the light.

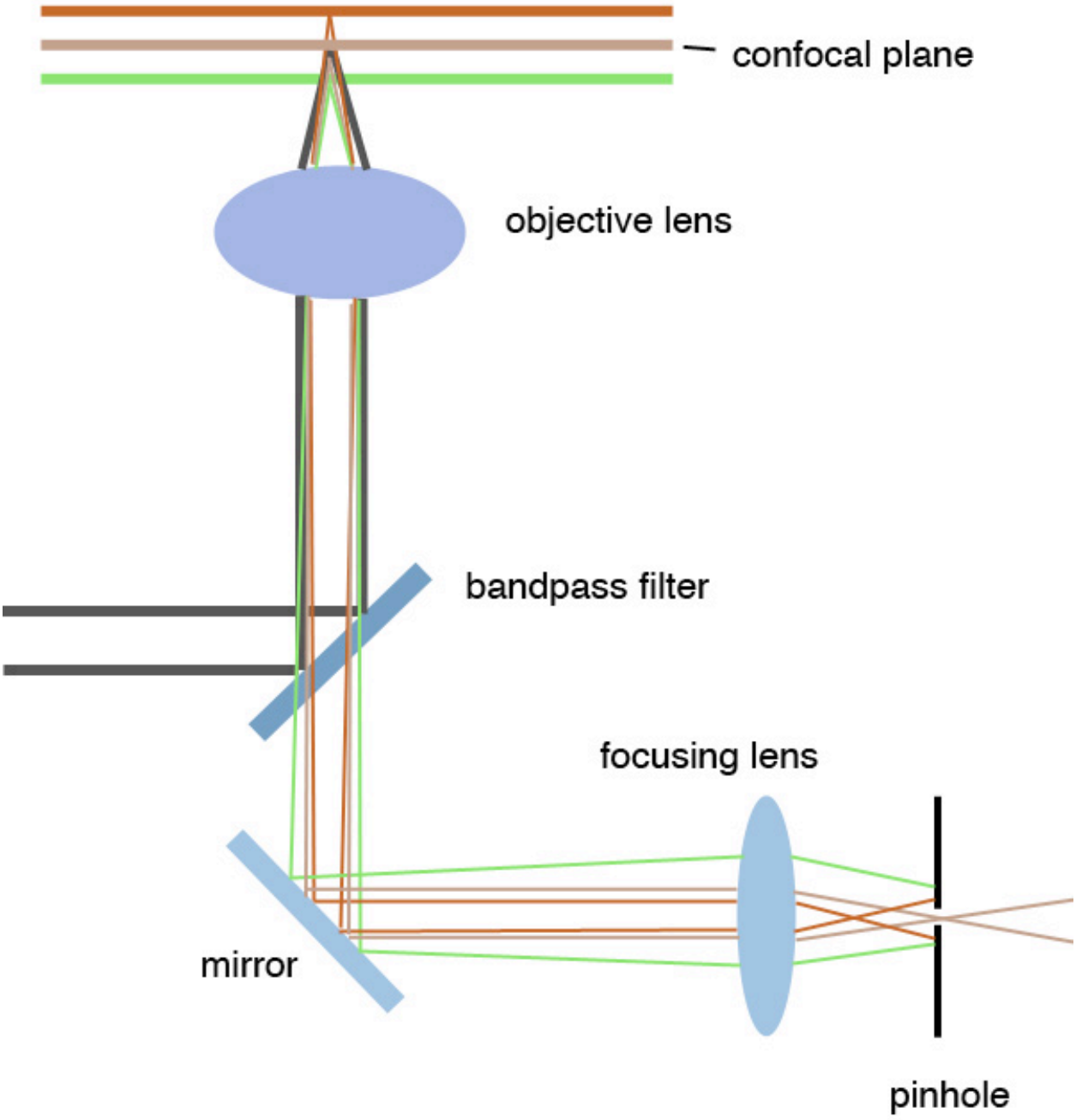

Figure 5: Schematic for a confocal setup

2.5 Time-correlated single photon counting

In order to unmix or resolve fluorophores by use of lifetime analysis, it is necessary to have temporal resolution of detected photons. Two different experimental techniques for fluorescence lifetime measurements are possible: time-domain and frequency-domain. The frequency-domain technique is reported to exhibit an error 1.5–2 times larger than that of time-domain [15], which is still acceptable for many applications. At larger photon fluxes, time-domain techniques are limited by pile-up, which is a form of electronic saturation, whereas frequency-domain techniques are only limited by the saturation of the detector itself [15]. As there is no need for high photon fluxes, and therefore no advantage to using frequency-domain techniques, the time-domain technique is used here in the form of TCSPC. This can then be applied to techniques such as FLIM or FRET [16]. The ability to tag each photon with the time delay since the preceding laser excitation pulse on a sub-nanosecond scale allows the sample's fluorescence lifetime to be found. Also, with the proper algorithms and equations, techniques can be formed that are much simpler in a visual sense to analyze the data. In particular, this can be seen in the AB-plots shown by Hanley to analyze FRET processes in the frequency domain [17].

For collection of signals from different emission wavelength bands, the signals from the four SPADs are combined through a router, which records which SPAD detects each photon. It is then possible to take the separate wavelength bands and view the time-

resolved contributions from each simultaneously, thereby providing a data set from which the fluorophores can be linearly unmixed, as discussed in Section 2.7. The technique of recording a time and spectrally resolved data set using TCSPC (but without linear unmixing of contributions from different species) is reported in reference [14].

2.6 Prism spectroscopy and interference filters

A spectrally resolved image shows at each pixel of the image the intensity for each band of emission wavelengths. For acquiring the data, many techniques can be used, including wavelength scan, spatial scan, time scan, and various other methods. In the wavelength-scan method, a whole image is measured one wavelength at a time. In a spatial scan method, a dispersion prism or diffraction grating is placed in the setup to separate the emission spectra, which is collected all at once. For collection of emission spectra in Fourier Transform spectroscopy, a time scan method is used, in which the image is measured after passing through an interferometer. A mathematical transformation, such as a Fourier transform, is then applied to the data to see the spectrum at each pixel [18]. One group has used the wavelength-scan technique by introducing a liquid crystal tunable filter. By establishing a spectral library, they were able to use the spectral information gathered to distinguish between closely related IFPs [19]. Due to the low speed of acquisition afforded by single-photon counting and the lack of added mathematical processes, a spatial scan method was chosen for this experiment. The microscope includes a 3-D piezo-stage for scanning the sample

position with respect to the confocal volume. However, for the purposes of studying linear unmixing of spectra with low numbers of collected photons, the spatial scanning is not used, and the collected data corresponds to that which would be acquired at a single pixel of an image.

Two experimental configurations are studied in the research for this thesis. In the first experimental setup, a Brewster prism is used to disperse the fluorescence. The prism is adjusted so that the incoming beam hits the prism face at Brewster's angle $\left(\theta_B = \arctan\left(n_2/n_1\right)\right)$, to ensure that the *p*-polarized reflection from the prism, according to Fresnel's equations, will go to zero. If the polarization of the incoming beam is oriented to be *p*-polarized, the loss of signal through the prism will thus be minimized.

The second experimental setup uses dichroic mirrors, which are longpass filters designed to reflect wavelengths below a certain design value. They consist of alternating layers of optical coatings on a glass substrate, which selectively reinforce the reflection of specified wavelengths of light while transmitting others. The thickness of the layers enables one to control the passband of the filter, hence they are available to reflect selected bands, or to simply act as longpass or shortpass filters.

2.7 Maximum-likelihood estimation

The unmixing of spectral data becomes important when the species involved spectrally overlap. The idea of linear unmixing has been reported earlier in remote sensing, where multiband images taken by satellites contain different components within the same scene. As the image information is distributed across several or all of the channels, methods have been derived to interpret the image as a whole, with linear unmixing being one of the ideas constructed [2]. As with any mathematical problem, one needs at least as many equations as there are variables in order to find a unique solution. In this case, the spectroscopic channels become the analog to equations as the contributions of each of the species in the mixture become the variables.

Two methods are primarily used for linear unmixing. These are nonlinear weighted least squares (LS) estimation and ML estimation. ML estimation is a rigorous method for fitting data in which it is assumed that a Poissonian distribution of photon counts occurs in each spectroscopic channel. Each variable has a set of possibilities that the algorithm iterates through, generating a potential fit for each possibility. The parameters that give the most probable fit to the given data are thus found. It is based on the concept of maximizing a likelihood function.

LS is generally the more popular estimation method for unmixing This form of analysis makes an implicit assumption that the statistical errors in the data exhibit a Gaussian

distribution. Weights inversely proportional to the Gaussian variance at each point may be applied. This assumption of Gaussian distributed errors is generally valid for analog detection of light. However, the LS method has no basis of constructing confidence intervals. MLE, on the other hand, can do this, as well as provide the following desirable properties:

> "sufficiency (complete information about the parameter of interest contained in its MLE estimator); consistency (true parameter value that generated the data recovered asymptotically, i.e. for data of sufficiently large samples); efficiency (lowest-possible variance of parameter estimates achieved asymptotically); and parameterization invariance (same MLE solution obtained independent of the parameterization used)." [20]

Maus *et al.* did a study comparing MLE and nonlinear weighted LS, to see which performed better when measuring the fluorescence lifetimes of single molecules. A total of 71 decay profiles were analyzed, ranging from 2500–60000 total counts in each. They found that the fit quality parameters of nonlinear LS are slightly below 1, indicating that there is improper weighting in the method. They also notice that the MLE method estimates lifetimes to be 5% larger than LS, resulting from a more appropriate weighting and fitting of the decay channel region with only a small number of counts in the MLE

case. As the total counts increase, the two methods begin to converge. They conclude that the “superior performance of MLE over LS in analyzing low signal-to-noise fluorescence decays as found experimentally here is not only important for single-molecule spectroscopy but for all other low signal applications of time-resolved fluorescence spectroscopy.” [21]

Other methods have been attempted besides these two. One, based on the classical least square estimation, involves using neighboring pixels in a matrix form to find the information embedded in the pixel of interest. It is used for the purpose of remote sensing [22].

In related work, Enderlein *et al.* developed MLE methods for their work in 1996 to distinguish different types of molecules at the single-molecule level based on their fluorescence decay measurements. As the time-resolved fluorescence measurements for Rhodamine 6G (R6G) and tetramethylrhodamine isothiocyanate (TRITC) molecules were analyzed, they became the first group to report single-molecule identification by fluorescence decay in a mixture. By first taking pure-sample measurements of both R6G and TRITC, then making a mixture of the two dyes, they identified and counted single molecules of each species within the mixture to find the expected ratio of molecular species in the mixture. They found the following:

> "We demonstrated the efficiency of the ML estimator for identifying single molecules using TCSPC measurements. For the small numbers of processed bursts, the comparison with theoretical predictions is satisfactory. By improving the photon detection efficiency in SMD experiments, it should be possible to decrease significantly the error rate for single molecule identification." [23]

Some groups, such as Hoppe *et al.* [24], have combined several techniques in an attempt to increase accuracy in their linear resolution. In their work on three-dimensional FRET microscopy reconstruction, they have included ML estimation by entropy maximization, LS minimization by steepest and conjugate gradient descents, the iterative constrained Tikhonov-Miller algorithm, and conjugate gradient minimization of maximum a posteriori functionals. Although computationally rigorous, it yields superb results when applied properly [24].

Chapter III

Data analysis methods

In this chapter, a discussion is made on how data from an experiment is prepared and analyzed. The mathematics behind unmixing is explained in depth. MLE methods, which were briefly introduced in Section 2.7, are investigated further.

3.1 Mathematics of unmixing

The most commonly used method to separate individual species in spectral imaging is weighted LS estimation (see Section 3.2). It is the routine used by the commercial microscope devices discussed in Section 2.1. Although it gives very respectable results in most cases with multiple fluorescent species present, it fails at low photon counts. This is due to its assumption of a Gaussian distribution of photon counts within each channel. As is well known, photon statistics exhibit a Poissonian distribution. In order to apply statistically rigorous unmixing techniques to an experiment for the low photon counts of an ultra-sensitive regime, a different method must be implemented. The technique chosen here is that of the MLE method, which will be presented in Section 3.3.

3.2 Weighted least squares unmixing

As previously stated, weighted least squares is a commonly used method of unmixing. The reason it is not used here is because as the photon counts get less, in the range of 100 photons, it systematically underestimates the error by ~5%. When the counts drop below ~100 in any spectroscopic channel, it gives inaccurate results. One starts with the following as a basis:

$$\chi^2 = \sum_{i=1}^{n} w_i \left(y_i - f_i(x_i; a_1, ..., a_k) \right)^2, \quad (1)$$

with $w_i = 1/\sigma_i^2 = 1/y_i$. (2)

The quantity χ^2 is the value that is to be minimized by adjustment of the fitting parameters $a_1, ..., a_k$. It consists of the sum over all *n* spectroscopic channels of the weighted residues, i.e., the differences between the number of photons y_i in the spectroscopic channel x_i and the value of the fitting function in that channel, $f_i(x_i; a_1, ..., a_k)$. It is multiplied by the weighting term, made up of the reciprocal of the variance, which for Poissonian photon statistics equals the number of detected photons. The different spectroscopic channels x_i include those obtained from different SPAD detectors for the different emission wavelength bands, for each of the different time delays following a laser excitation pulse, as collected by the instrumentation for TCSPC (i.e., by the Picoquant Time Harp 200). (That is, all differences in spectroscopic information are represented in one-dimensional form.)

For linear unmixing, the fitting function takes the following form:

$$f(x_i) = \sum_{j=1}^{k} a_j s_j(x_i) + b(x_i), \quad (3)$$

where a_j are the estimated numbers of photons from each of the k fluorescent species. These have normalized spectral signatures $s_j(x_i)$, which are collected in calibration experiments. The term $b(x_i)$ is the expected background in each channel.

Weighted least squares fitting fails when there are low numbers of detected photons in any given spectroscopic channel. For example, in the case where there are no photons detected, the Poissonian error in the number of detected photons is also zero and the weight at that point, given by Eqn. (2) is then infinite. If there are no photons detected in any one spectral/temporal channel of the data set, the corresponding infinity from Eqn. (2) is enough to skew all the results of the unmixing algorithm.

3.3 Maximum-likelihood methods

MLE is more rigorous than the weighted least squares methods and hence is more accurate when applied to data with low photon counts. It explicitly accounts for the Poissonian statistics of the number of detected photons. In the following paragraphs, the method is stated as it is implemented into a C++ algorithm used to unmix simulated or real data.

The program begins by reading in data from files (or by generating simulated data) and assigning the data to arrays as such:

$$m_i = \left(m_1, m_2, ..., m_n\right); \tag{4a}$$

$$m_i^{(j)} = \left(m_1^{(j)}, m_2^{(j)}, ..., m_n^{(j)}\right), \quad j = 1, ..., k; \tag{4b}$$

$$b_i = \left(b_1, b_2, ..., b_n\right). \tag{4c}$$

The individual terms m_i, $m_i^{(j)}$ and b_i are elements of arrays that represent the photon counts in each of the *n* spectroscopic channels (i.e., each emission wavelength band and temporal channel) for the mixture, the $j = 1, ..., k$ individual species, and the background, respectively.

In the analysis, the total numbers of photons for each data set are needed, so they are evaluated as follows:

$$M = \sum_{i=1}^{n} m_i; \tag{5a}$$

$$M^{(j)} = \sum_{i=1}^{n} m_i^{(j)}; \tag{5b}$$

$$B = \sum_{i=1}^{n} b_i. \tag{5c}$$

The background counts are found by acquiring photon counts with nothing but water as the sample for the same data collection time as used for each of the $j = 1, ..., k$ known species.

In order to provide calibration curves, the data sets for the individual species are normalized:

$$s_i^{(j)} = \left(m_i^{(j)} - b_i\right) \Big/ \left(M^{(j)} - B\right). \tag{6}$$

The variables to be optimized are then introduced:

$$\mathbf{f} = \left(f^{(1)}, f^{(2)}, ...\right), \tag{7}$$

where $\mathbf{f}$ is a 1D array that represents the fractional contributions of each of the *k* species in the mixture. An important thing to consider is that the components of $\mathbf{f}$ must sum to 1. With the $\mathbf{f}$ values, the total photon counts for the mixture, and the *s* values, a fit is constructed. The expected number of photon counts in the *i*-th spectroscopic channel is the sum of two components— the contribution from fluorescence and the contribution from background:

$$\mu_i = \left(M - B \cdot \frac{t_M}{t_B}\right) \cdot \sum_{j=1}^{k} f^{(j)} s_i^{(j)} + \frac{t_M}{t_B} \cdot b_i, \tag{8a}$$

where t_M is the data acquisition time for the mixture and t_B is that for the background. As the acquisition time for the background may differ from that for the mixture, the ratio $\frac{t_M}{t_B}$ is formed that adjusts the contribution from background to that expected in the acquisition of data for the mixture.

As has been explained in Section 2.3, a count-rate dependent time shift occurs in the TTL pulses of the SPAD detectors. Four extra adjustable parameters are introduced in the data analysis program to account for the possibility of different time shifts for each of the four SPAD detectors between the spectra of the individual species and the measured spectrum of the mixture. The analysis with accounting for this time shift may be expressed as the following equation for the expected number of photon counts in the i-th spectroscopic channel:

$$\mu_i = \left(M - B \cdot \frac{t_M}{t_B} \right) \cdot \sum_{j=1}^{k} f^{(j)} s_{i-\Delta_i}^{(j)} + \frac{t_M}{t_B} \cdot b_{i-\Delta_i}, \qquad (8b)$$

where

$$\Delta_i = \begin{cases} \Delta_1, & i = 1,...,n/4 \\ \Delta_2, & i = 1 + n/4,...,n/2 \\ \Delta_3, & i = 1 + n/2,...,3n/4 \\ \Delta_4, & i = 1 + 3n/4,...,n \end{cases}$$

Once all the arrays have been created and initialized, the ML method is implemented as follows: The probability (or likelihood) to obtain the data set measured for the mixture, $m_i = (m_1, m_2, ..., m_n)$, given that the fractional contributions are $\mathbf{f}$ and that the counts in each spectroscopic channel follow Poissonian statistics is given by:

$$L(\mathbf{m};\mathbf{f}) = \prod_{i=1}^{n} \left\{ \exp\left[-\mu_i(\mathbf{f}) \right] \cdot \mu_i(\mathbf{f})^{m_i} / m_i! \right\}. \qquad (9)$$

The fractional contributions $\mathbf{f}$ must be adjusted to maximize $L(\mathbf{m};\mathbf{f})$. In order to convert the product into a sum for faster computational evaluation, the natural logarithm of $L(\mathbf{m};\mathbf{f})$ is taken, giving the logarithmic likelihood function:

$$S(\mathbf{m};\mathbf{f}) = \sum_{i=1}^{n} m_i \ln \mu_i(\mathbf{f}) - \mu_i(\mathbf{f}) - \ln(m_i!). \tag{10a}$$

The last term can be dropped as the natural log of $(m_i!)$ is a constant throughout each iteration of $\mathbf{f}$. Hence, the quantity to be maximized in the algorithm is:

$$S'(\mathbf{m};\mathbf{f}) = \sum_{i=1}^{n} m_i \ln \mu_i(\mathbf{f}) - \mu_i(\mathbf{f}). \tag{10b}$$

The maximum is found by changing $\mathbf{f}$ in each run and saving the values of each component of $\mathbf{f}$ when a new maximum is found, i.e., the algorithm searches through a grid of possibilities for $\mathbf{f}$ until the maximum is found.

3.4 Testing the MLE unmixing method

Before this algorithm is used in an actual experiment, it is a good idea to simulate the experiment and see how the method performs. For this purpose, a Monte Carlo simulation has been created that takes parameters provided by experimental data, randomly generates a spectrum of a mixture, and then separately unmixes it. A version of the Monte Carlo simulation and data analysis software created in this thesis research is published online [28] and results from an earlier simulation are reported in Reference [1].

Monte Carlo methods were originally formed to model phenomena with stochastic processes. They generally incorporate computational algorithms based on random numbers to create simulations of systems with many coupled degrees of freedom. In the present case, the simulation models Gaussian-shaped prompt curves, which are convolved with exponential decays to produce fluorescence decay profiles. It simulates a spectral image, creating a multi-dimensional image of the brightness as well as a pixel-by-pixel temporal spectrum. Pseudo-random numbers are used to add Poissonian shot noise to the numbers of photons in each spectral/temporal channel. Again using random numbers, it is also possible to create simulated electropherograms, which are patterns of fluorescence bands that would be found as the output of an experiment for chemical separation by electrophoresis.

The code takes a straightforward approach to creating a simulated experiment. First, bins of expected fluorescence for known species are introduced. Lifetimes of the species can then be created by randomly populating the bins, thus maintaining a realistic ratio of one species to another if they were to be in a mixture. This simulated data may be saved to hard disk or analyzed by the steps explained in Section 3.3, to produce fractional contributions for the species present. To check how well the method performed, two error bars are created. One graphs the Poissonian likelihood function, $L(\mathbf{m};\mathbf{f})$ while the other checks to make sure that the confidence of the results is within a specified limit.

Chapter IV

Experiment

This chapter introduces the experimental setups, along with what is used to gather the data and how it is handled. Also discussed are alignment procedures and troubleshooting for data collection. Two experimental set ups have been studied in this thesis research. With the goal to create a high-throughput system with spectral dispersion, the first experimental set up included a low-loss Brewster prism, which acts as a spectrometer. However, due to problems with the design that led to poor optical coupling of the fluorescence light onto the detectors, it was replaced by the second experimental set up, which is based on dichroic filters. Both of these components are briefly discussed in Section 2.6. Their applications to an experimental setup are explained in greater detail in the following subsections. One main thing to keep in mind, referring back to the goals set forth in Section 2.2, is that the setup must incorporate a high-throughput layout that maximizes fluorescence collection to achieve ultra-sensitive detection.

4.1 Excitation laser and optics

The excitation laser and optics are common to both the prism and the dichroic filter experimental configurations and hence these are discussed first. The lasers and optical configuration described in this section were in place prior to this thesis research,

whereas the subsequent optical configurations described in the sections below were built as part of this thesis.

An excitation beam of 608 nm is generated from a dye laser (Coherent 700 dye laser operating with Kiton Red dye), which is synchronously pumped by a 2W, 76 MHz, 1 ps, modelocked 532 nm laser (SpectraPhysics Vanguard 2000-76MHz HM532). Another dye laser operating with DCM-Special dye is also available and is used during optical alignment. The output beam from the dye laser is first passed through a bandpass filter to remove weak broadband fluorescence emission inherent in the dye laser. During its path to the objective and sample on the coverslip, the power of the beam, typically on the scale of 10 mW, is attenuated to 600 μW. Larger laser power yields intensities that would saturate the fluorescence excitation and increase photobleaching of the dye molecules in the sample.

Photographs of the first experimental configuration are shown in Figures 6a-6d. In Figure 6a, the coverslip for the sample, as well as the pinhole for the confocal microscope are seen. The Brewster prism is shown in Figure 6b. The mirrors for separation of the spectral bands to their respective detectors are shown in Figure 6c. The setup as a whole, including the detectors and the housing to protect ambient light from entering the system, are seen in Figure 6d.

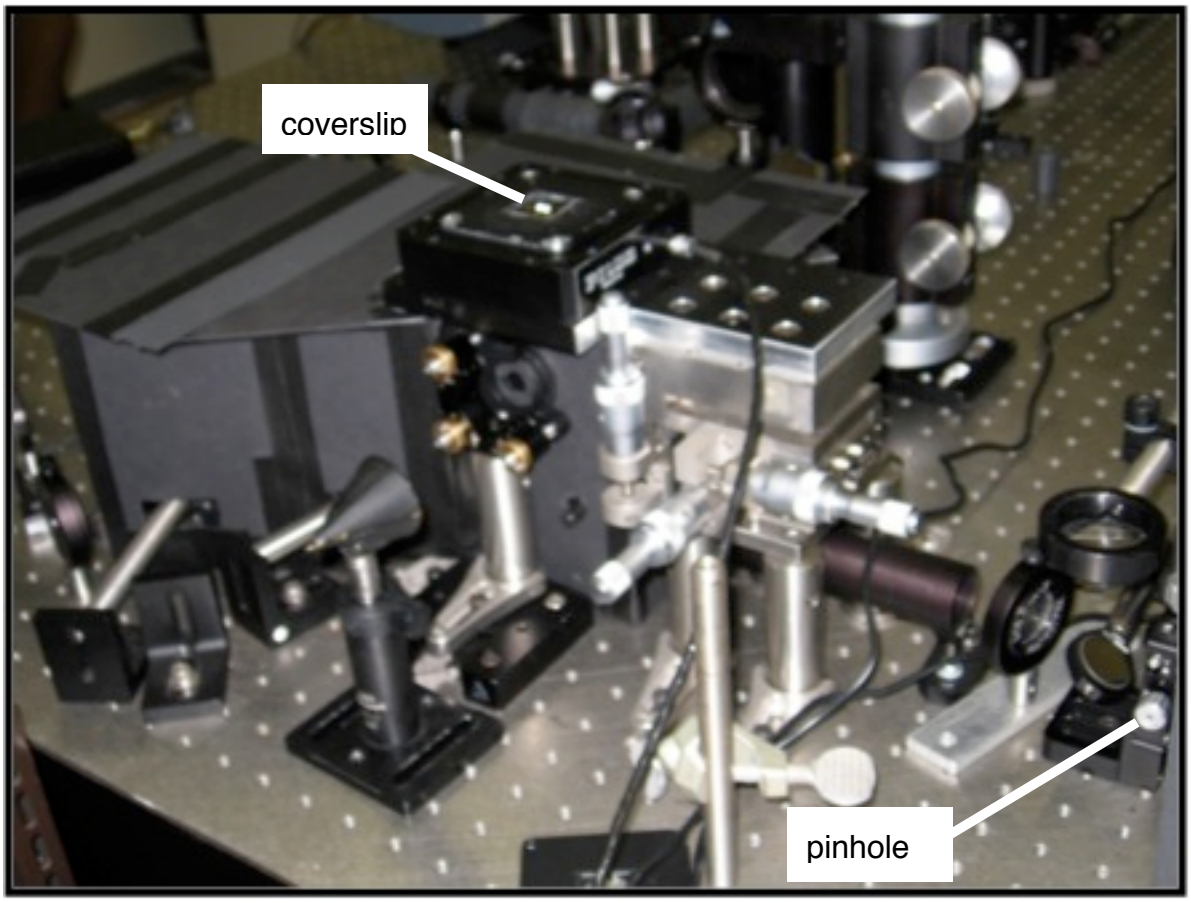

Figure 6a: View of coverslip for confocal microscope in setup

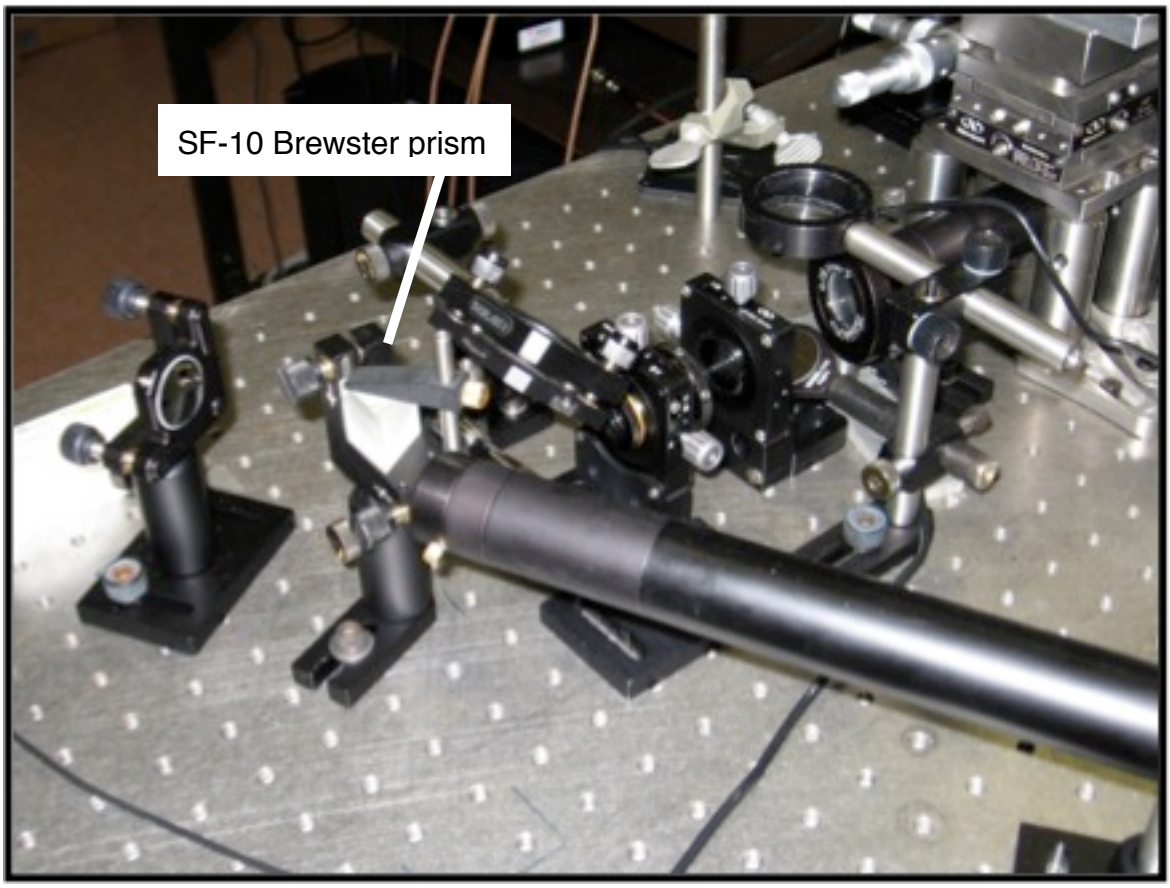

Figure 6b: Brewster prism and focusing lenses

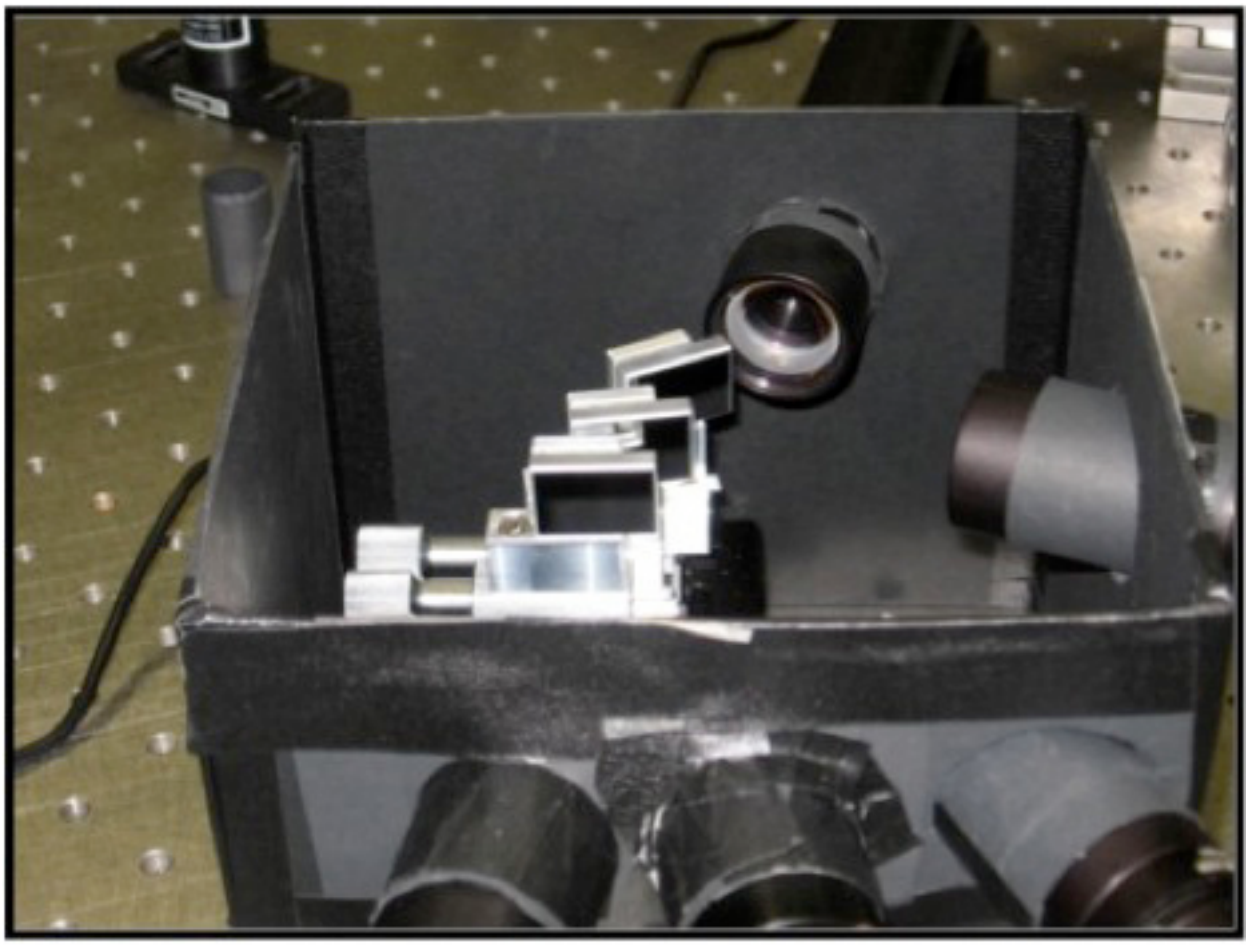

Figure 6c: Mirror mount that systematically picks of selected wavelength bands to the series of detectors

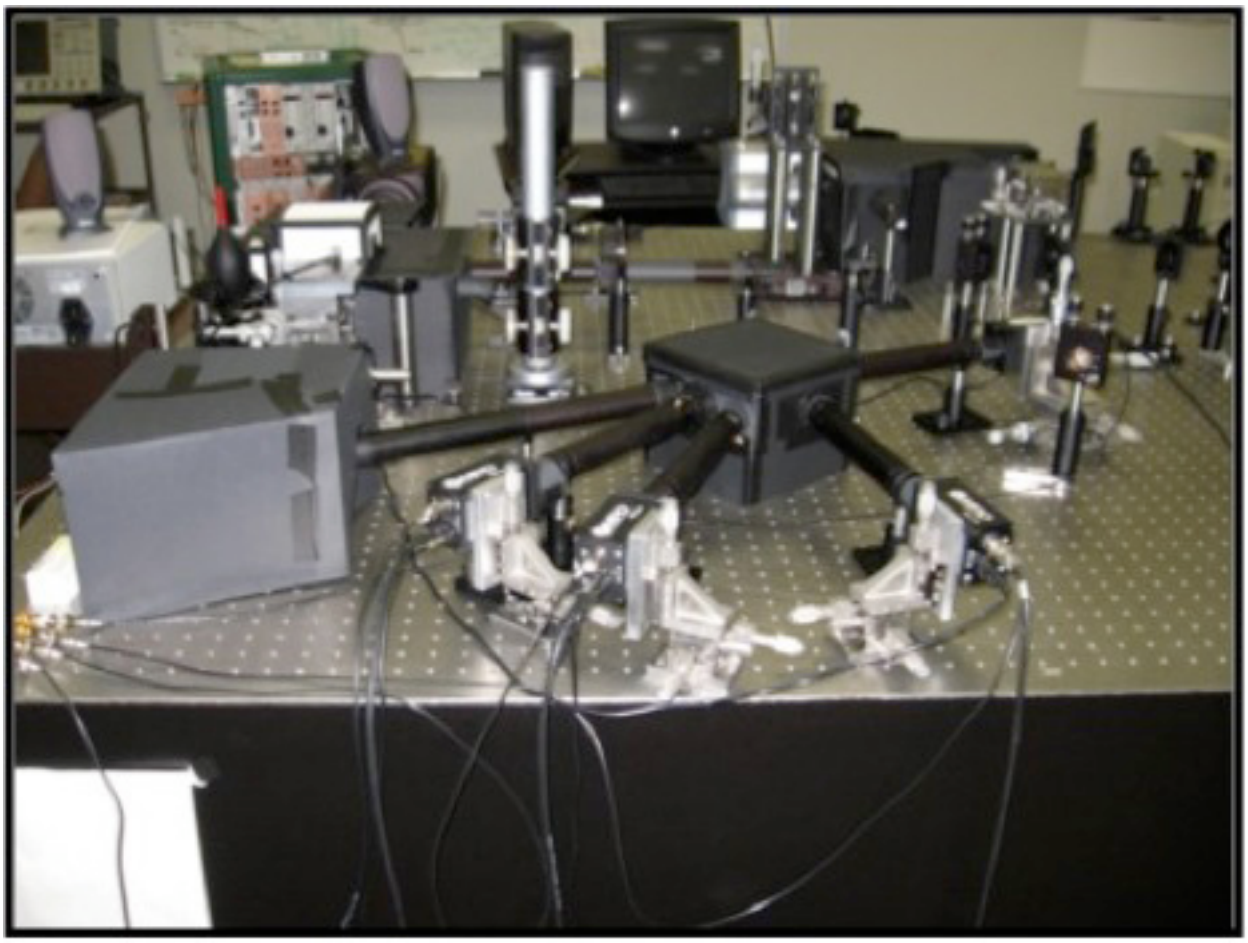

Figure 6d: View of entire prism spectroscopy-based setup

Approximately 10% of the beam reflects from an uncoated fused-silica substrate (shown in Figure 5) and then enters the objective (Olympus UPlanApo 60x/1.2w ∞/0.13-0.21) and is focused onto the top surface of the coverslip. A translation stage is then used to adjust the position of the coverslip so that the beam focuses 50 μm above this surface, inside the sample. The fluorescence is collected by the same objective and the beam of fluorescence light then exits with a 9 mm diameter (the exit pupil diameter of the objective). It passes through a holographic Raman notch filter (Kaiser Optical Systems) that blocks 608 nm wavelengths and hence removes the elastically scattered laser excitation light from the beam. This beam of fluorescence light is then focused to a 150 μm pinhole, which acts as a spatial filter for the confocal microscope.

4.2 Prism configuration

After the pinhole, the beam of fluorescence light expands to another lens, slightly offset from where it would collimate the beam so as to focus to a set of mirrors, as seen in Figure 7. Immediately after the lens, the beam passes through a Brewster prism made of high dispersion SF-10 glass. This provides spectral dispersion and expands the signal out into a spectrum, which is picked off by the mirrors to specified wavelength bands. In this case, the bands are centered at 620 nm, 640 nm, 660 nm, and 700 nm. Provided that the polarization of the beam of fluorescence is preserved in the horizontal plane, Fresnel loss from the prism would be minimal and maintain optimal photon throughput, but fluorescence that is vertically polarized suffers Fresnel loss at the prism

surfaces. Each path for the separate bands goes through a spherical concave mirror to expand the beam further and fill the area of the focusing lens placed before the detectors. This is also seen in Figure 7.

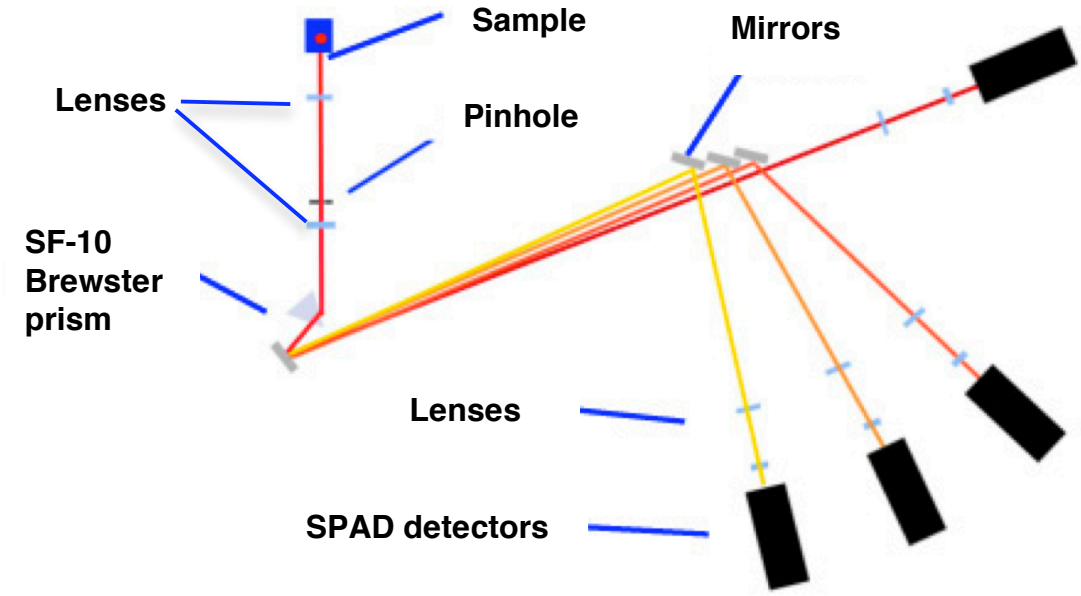

Figure 7: Schematic of original layout

The prism spectrometer setup was unable to achieve the desired high throughput of collected fluorescence, because the fluorescence could not be focused onto the small active area of the SPAD detectors. As the beam hits the concave lenses, it is still expanding in the horizontal axis from the Brewster prism. This causes the signal from wavelengths outside the one in which the path is centered to be expanded to an elliptical beam at the focusing achromat. Those wavelengths of the beam that enter the

edges of the achromat are skewed as they do not pass through the center of the concave lens. This gives rise to coma and aberrations in the focusing of the beam at the SPAD detector, which has an active area of only 150 microns diameter. Because of this, much of the signal is lost.

One possible way to alleviate this is to rearrange the optics to allow for proper focusing at the detector. However, this was not attempted due to time contraints and the necessary optics were not be available in the lab. Another solution could be to add a second Brewster prism between the first and the detectors to re-collimate the beams of fluorescence, as shown in Figure 8 and as performed in Reference [1]. The spectra would be dispersed and collimated by the time it reaches the mirror mount. This ensures that the spectral bands reflected to the detectors will be expanded properly by the concave lenses and focused tightly onto the active area. However, there is a disadvantage in this approach in that there are now four prism surfaces that incur Fresnel loss for the p-polarized light, and this defeats the goal of high-throughput signal. Hence, in order to achieve high throughput, a second experimental configuration based on dichroic filters was set up.

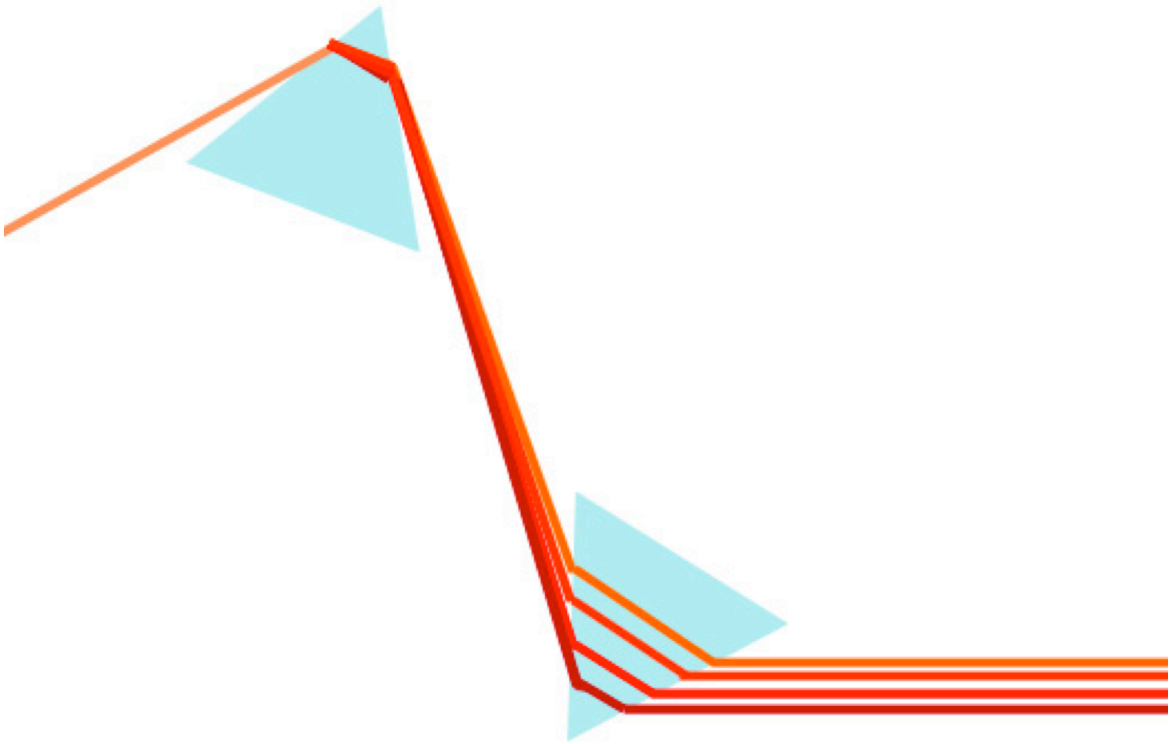

Figure 8: Possible two prism setup

4.3 Interference filter configuration

The second experimental setup is based on the use of dichroic filters to separate the beam of collected fluorescence into four bands. The configuration is seen in Figure 9 and in the full schematic in Figure 10. After passing through the pinhole, the beam is collimated with a lens. It is then passed through a series of three dichroic mirrors, each with a different cutoff wavelength. The bands are similar to the ones before, except that the path centered along 620 nm collects all wavelengths below a value of around 630 nm rather than a small band. The path centered along 700 nm similarly collects all the wavelengths above about 675 nm. This should not be an issue for the 620 nm path, as the emission rarely dips much lower than 590 nm with a signal that is significant. An issue does occur, however, with the 700 nm path, as there is Raman scatter from water in this beam of fluorescence, which affects the count rate. This additional prompt component is calculated to be around 675 nm, just inside the range for the 700 nm band. The calculation of this Raman shift is done with the equation $hv = h(v_o - v')$ where v is the new wave number after the shift, v_o is the wave number from the initial wavelength, and v' is the shift caused by Raman scatter in water. In this case, $v_o = 1/(608nm)$ and $v' = 1643.5m^{-1}$ [25]. Solving for v, one finds it is 675 nm. It can be assumed that this offset is constant throughout the samples and therefore should not hinder the separation and identification of the dyes.

The signals of each path are focused by 10x microscope objectives to the custom-modified SPAD detectors, which are briefly discussed in Section 2.3 and later in Section 4.5. The output signals generated by the incoming photons are then sent to a TCSPC module (Picoquant TimeHarp 200 with PRT 400 router). This provides lifetime curves and temporal data for the emitted spectra, which are later analyzed by a computer algorithm to linearly resolve the fractional components of the dyes.

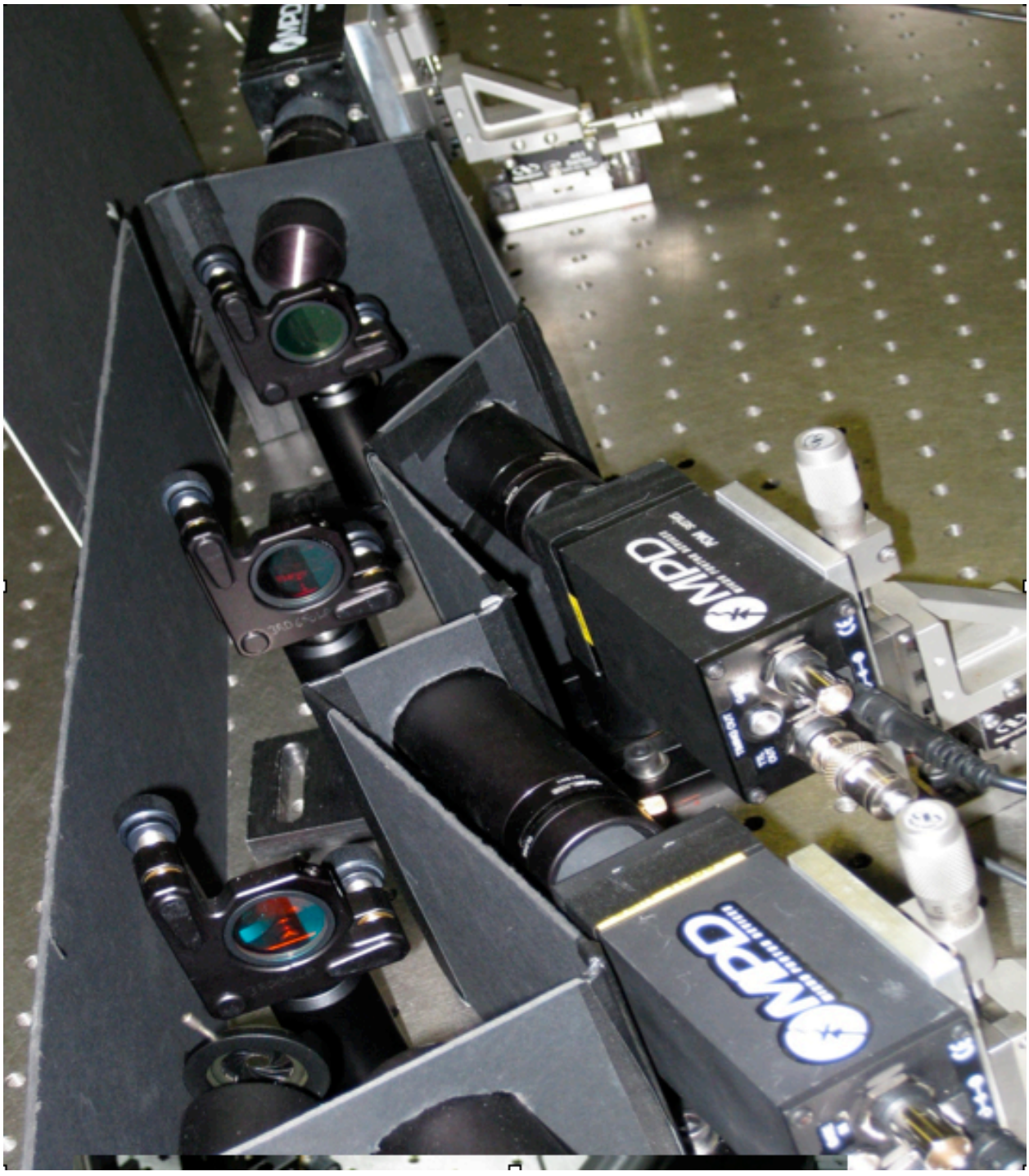

Figure 9: Current setup using dichroic mirrors

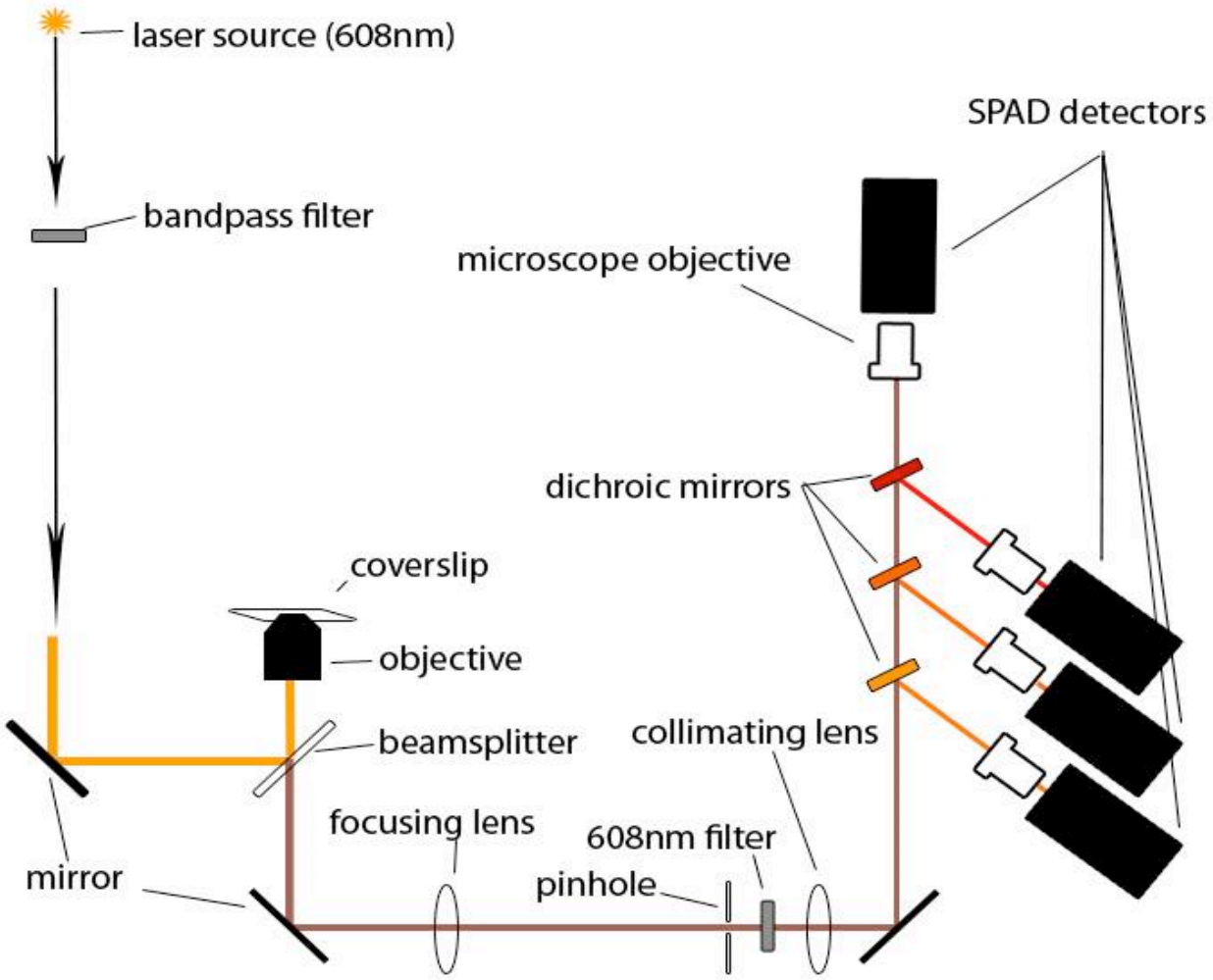

Figure 10: Schematic of new layout

4.4 Alignment

One aspect to keep in mind is having the setup well aligned. For the prism setup, the two dye lasers were first adjusted to emit at 620 nm and 660 nm. The beams are combined to one collinear beam at a beam splitter, which enters the microscope and is reflected off the top surface of the coverslip, so that it follows a path through the pinhole to the prism. The two colors are the separated and take separate paths to the mirrors, which can be adjusted to pick off the laser light and reflect it to each beam's corresponding detector. A mirror before the Brewster prism is then turned so that the beam from the 620 nm path enters the 660 nm path. This shift puts the 660 nm beam along the 700 nm path, which then allows that detector to be aligned. Finally, one of the dye lasers is tuned to 640 nm to align the last mirror, thus centering the last detector.

The setup with dichroics filters is aligned systematically by first placing and aligning the 700 nm band detector. Then dichroic mirrors and their respective detectors are placed in decreasing order of wavelength, from 660 nm to 640 nm to 620 nm. Reflected laser light from the tuned dye lasers is used to give a general alignment for the detectors. As the paths are now defined for both layouts, a sample of moderately concentrated dye, 100 nM Alexa 610, is put on the coverslip. The excitation beam, now back to 608 nm, is focused into the sample so that the detectors can be adjusted to get a maximum count rate for the fluorescence. Once this is done, the alignment process is completed and the setup is ready to start acquiring data.

4.5 Electronics and data file structure

With the optical layout complete, it is important to consider the electronic devices involved in the experiment that will allow for spectral detection with temporal resolution. As described in Section 2.3, SPADs are the most appropriate choice for an experiment of this type. Section 2.3 also explains that the detectors used in this setup are custom modified to proved stable sub-nanosecond timing and a higher QE in the deep red region of the spectrum. The increased QE in the red is an advantage in that the dyes typically used in fluorescence microscopy emit in that spectral region. The stable sub-nanosecond timing allows for better spectral resolution. In turn, this allows the lifetimes of the samples to become a parameter in the unmixing of the contributions from the fluorophores that are present.

As seen in the optical setup (Section 4.3), TCSPC modules are used to route the signals produced from the four SPAD detectors. These can run in two separate modes, specified before data acquisition. They can either determine and histogram the photon arrival times with respect to a sync signal from a photo diode powered by the 76 MHz laser pulses. The fluorescence lifetime of the sample can then be determined from the histogram. The histogram can be exported to a text file and then sent to a C++ executable that reads in the files and applies a maximum-likelihood algorithm to spectrally resolve the fluorophores into their fractional contributions.

The other way of collecting data is the “time-tagged time-resolved” (TTTR) mode, which stores the data as a “.t3r” file. This is a binary file with a particular format. Each record of data includes the time of arrival for the photon with respect to a 100 ns internal clock (the macro time), the time with respect to the prior laser pulse sync-signal with 34 ps quantization (the micro time), and which SPAD channel the photon signal came from (the router information).

A Labview program with C dll library calls was created as part of this thesis research to read in the “.t3r” file record-by-record, so that a desired number of photons or data collection duration may be analyzed. Hence the program splits the files to see the relevant data, then combines them into the maximum-likelihood algorithm so the MLE method can once again find the fractional contributions to each fluorophore in the sample. The advantage to this method is that a macro-time window can be adjusted after the data has been collected to select the number of photons that are passed to the ML analysis. This aids in evaluation of the ML method for varying levels of signal, i.e., for varying numbers of photons.

Long data collection runs for each individual fluorophore must be gathered to be normalized and give the fingerprint spectral profiles for the unmixing process. A run for the background must also be acquired to allow for proper calibration of the individual

dyes and the mixtures created. Different quantities of dye mixtures are also be used to provide linear trends for concentration patterns, as discussed in Section 5.2.

Chapter V

Experimental Results

In this chapter, results from experimental data are analyzed and discussed. The chapter first explains how the dye solutions are created and prepared for use in the experiment. Once they are prepared, concentrations are prepared that allow for results that would correspond to mixtures investigated by previously reported Monte Carlo simulations [1]. As the experiment and dyes have been assembled, data is acquired and analyzed. Expected results are calculated to give an accuracy check to the experimentally fitted data. These values are then compared and shown graphically. Finally, discussion is given on the possible sources of errors and what can be done to reduce errors.

5.1 Sample Preparation

The dyes used for the experiments in this thesis are Texas Red, Alexa 610, and Alexa 633. The dyes were made by diluting solutions, bought from Invitrogen, with water, and then analyzed in a spectrometer to find their absorbance. From this and their extinction coefficients, the concentrations of the stock solutions of the dyes can be calculated and then diluted as necessary. The formula used is the Beer-Lambert Law:

$$A = \varepsilon l c , \tag{11}$$

where A is the absorbance (dimensionless) , ε is the extinction coefficient or molar absorptivity (in L mol^{-1} cm^{-1}), l is the path length (in cm), and c is the concentration (in mol L^{-1}).

With the use of the emission and excitation spectra of each dye, downloaded from the website of Invitrogen, the spectral behavior of the dyes if they are together in a mixture can be seen graphically in Figures 11 and 12. Figure 11 shows the absorption spectra of each dye and the 608 nm laser excitation wavelength.

Each dye is excited with a different magnitude at this wavelength. With this fraction known, the emission in each channel can be found with the assumption that the fluorescence quantum efficiencies are the same. These expected curves are seen in Figure 12. The emission spectra of each dye are separated into 4 bands, equivalent to those in the experiment (see Section 4.3).

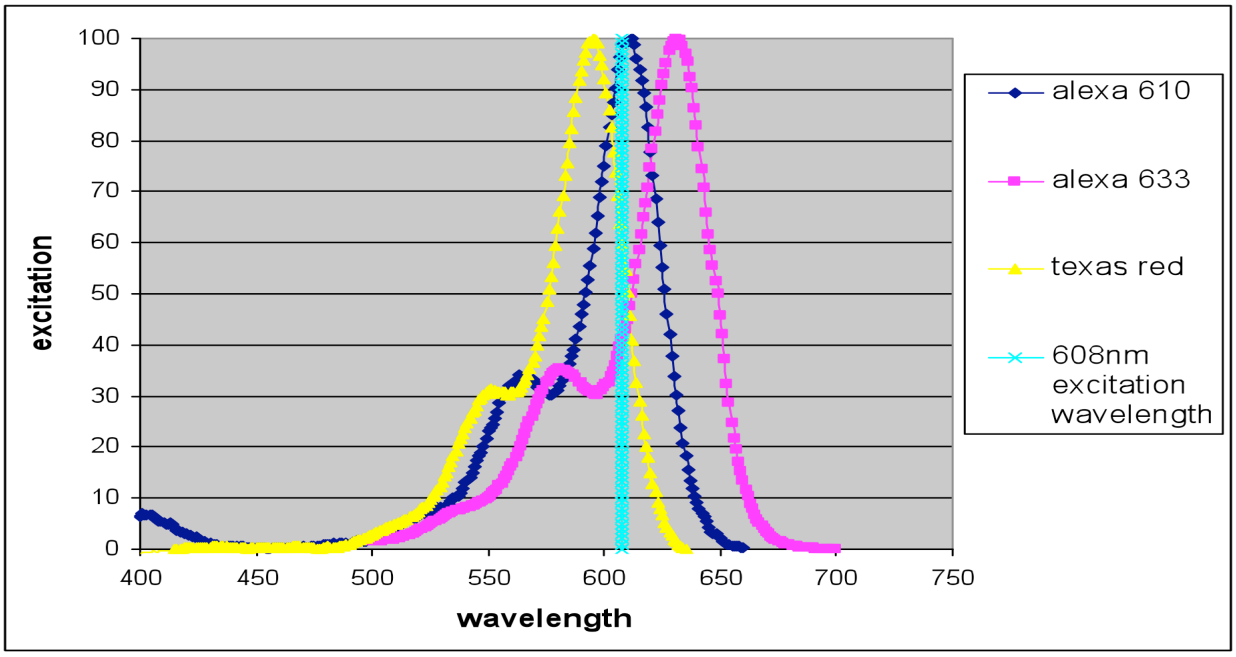

Figure 11: Excitation curves for dyes used in experiment, showing the 608nm laser beam will excite all three

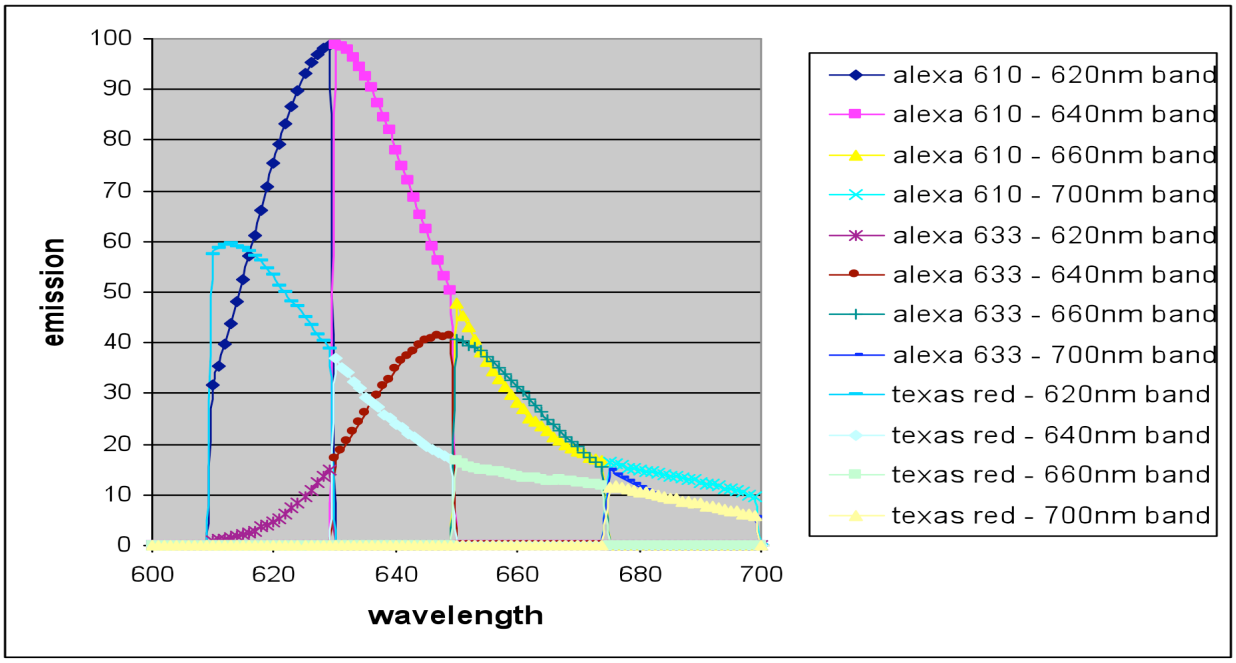

Figure 12: Emission bands in all four channels for the three dyes used in the experiment

By integrating the curves, the contributions of each dye in each separate spectral channel can be found. The result is seen in Figure 13.

Figures 11-13 show the theoretical combination of dyes given a normalized spectrum for each dye. For this reason, it is important to understand that only the magnitudes of the spectra are shown and that the dyes are not shown with equal concentrations.

The spectral unmixing also uses time-resolved data, to help unmix the contributions of dyes with different fluorescence lifetimes. Figure 14 shows the actual (unnormalized) calibration curves collected for the three dyes and for the background, which are used to find the normalized fingerprint spectra by use of Equation (6).

An average count rate of the dyes can be observed. This allows the dyes to be diluted to concentrations in a given range that give similar count rates. The concentrations used in the experiment are as follows:

Texas Red – 190pM	(1068 counts/s)
Alexa Red – 10pM	(2144 counts/s)
Alexa 633 – 188pM	(2257 counts/s)

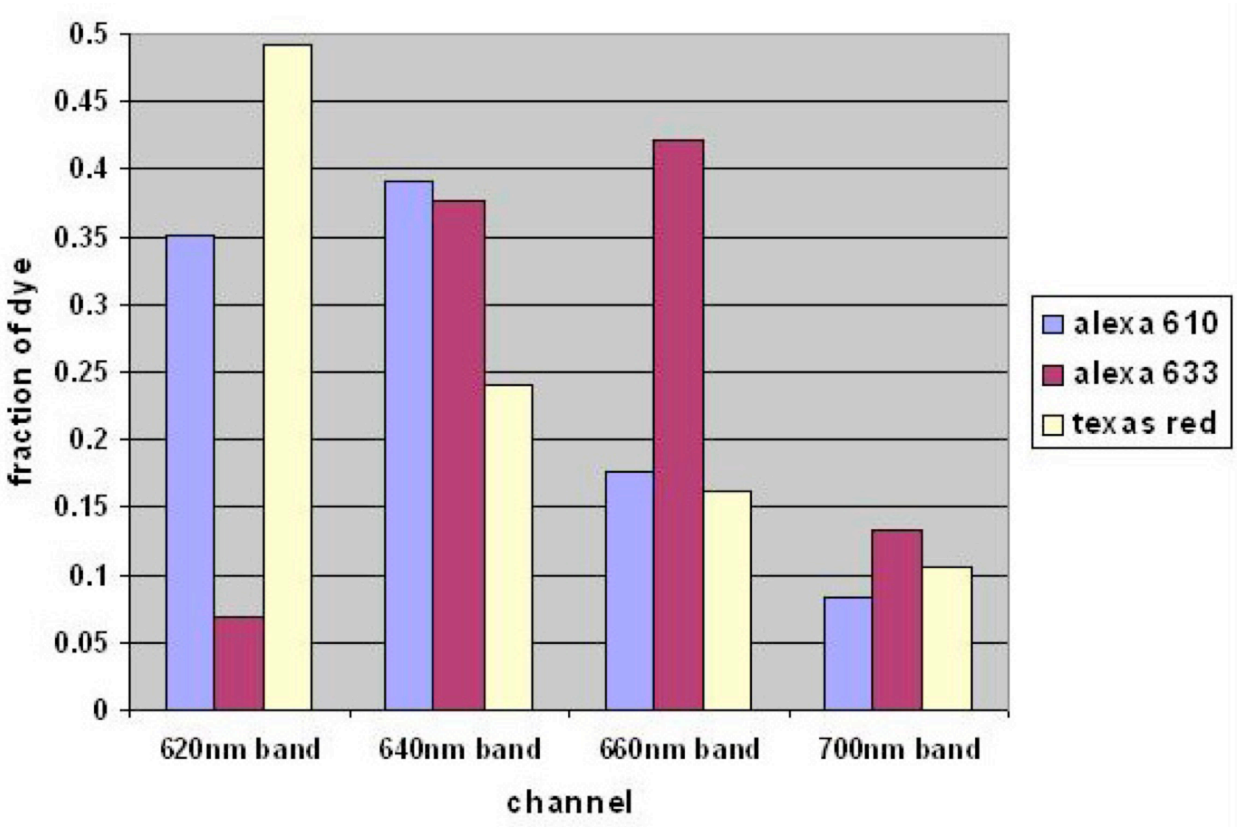

Figure 13: Contribution of each dye in spectral bands

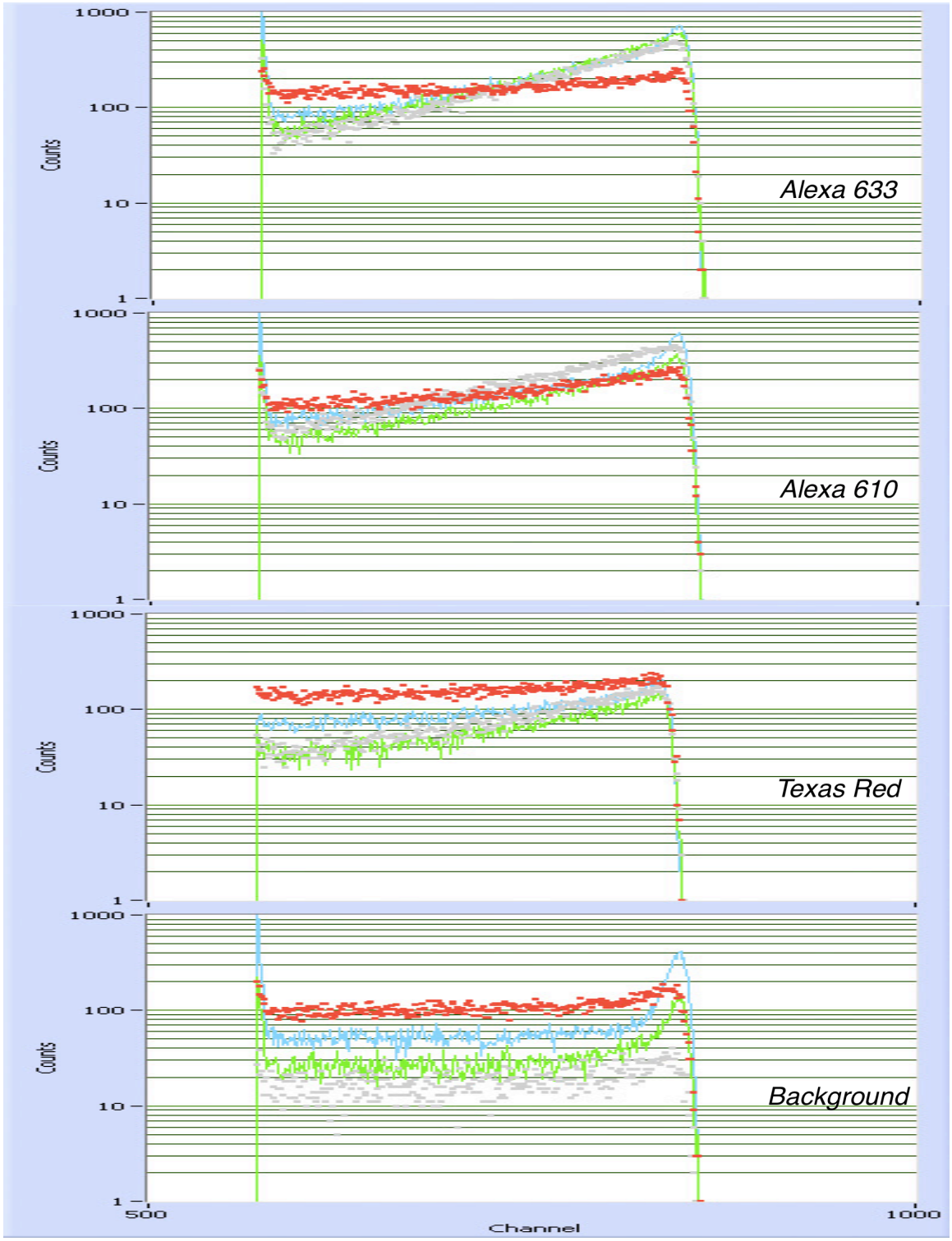

Figure 14: Contribution of each dye into separate bands

5. 2 Results and Discussion

As mentioned in Section 4.5, varying quantities of dye contributions need to be mixed and analyzed in order to obtain a set of results from which self-consistency in the analysis results can be demonstrated. This is desirable to check the validity of the method. Data was acquired for 17 separate runs at varying fractions of species. A constant volume was maintained in each run at 30 μL. Figure 15 describes these values and the length of the collection time for each run.

As can be seen in Figure 15, the first runs with single species have longer collection times than the mixtures. This is because the calibration curves to be used as ideal samples in the ML estimation need to be as precise as possible, as the MLE method does not account for shot noise in the fingerprint calibration spectra. In addition, shot noise can play a part in the acquired data, so shorter collection times for the runs to be unmixed aids in minimizing this influence. Further analysis indicates that an even longer collection time than used is desirable for the calibration curves to further reduce this effect.

collection time (in seconds)	Texas Red (µL)	Alexa 610 (µL)	Alexa 633 (µL)	Water (µL)
90	10	0	0	20
90	0	10	0	20
90	0	0	10	20
90	0	0	0	30
45	4	16	0	10
45	8	12	0	10
45	12	8	0	10
45	16	4	0	10
45	4	0	16	10
45	8	0	12	10
45	12	0	8	10
45	16	0	4	10
45	0	4	16	10
45	0	8	12	10
45	0	12	8	10
45	0	16	4	10
45	10	10	10	0

Figure 15: Combinations of dyes used for data collection

With Figure 15 as a guideline for forming the mixtures, data is collected and run through a Labview program to be unmixed within C dll files. A part of the front panel of the Labview vi can be seen in Figure 16. An example of the fit produced can be seen in Figure 17, with the residue of the experiment vs. fitted data shown in Figure 18. The residues are randomly distributed about the origin, which indicates a good quality of fit, within the precision afforded by the photon statistics.

The results compared to the expected values can be seen in Figures 19-22. In order to make these graphs, the expected contributions from each of the dyes within the mixture need to be derived. Two runs of 90 seconds each were taken for each calibration curve. The average number of counts found for each dye is found and then divided by the run time. This gives the count rate for the individual fluorophores. The data acquired in the experiment for the pure samples inherently has background present. It is thus already accounted for and does not need any further attention.

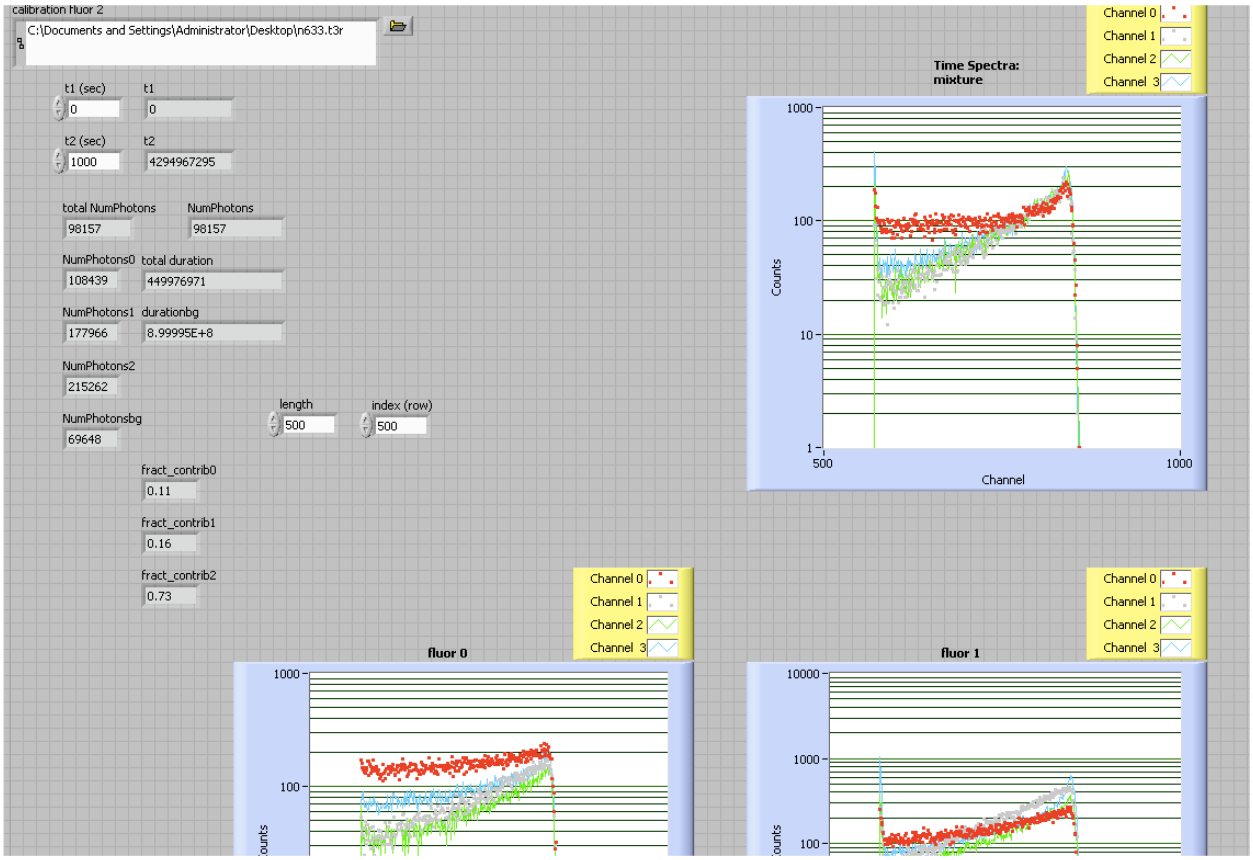

Figure 16: Screenshot of Labview program, demonstrating the output

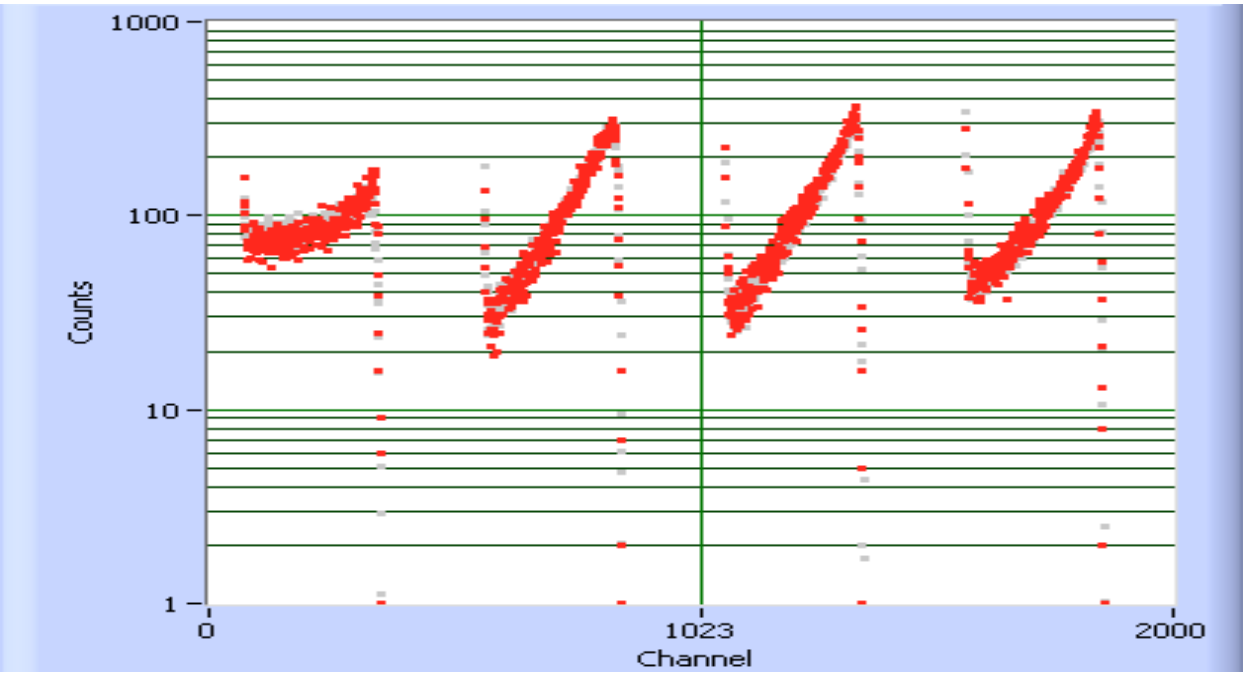

Figure 17: Fit (gray) vs. measured mixture (red) from Labview program. In this figure, results for 12 µL of Texas Red and 8 µL of Alexa 633 are shown.

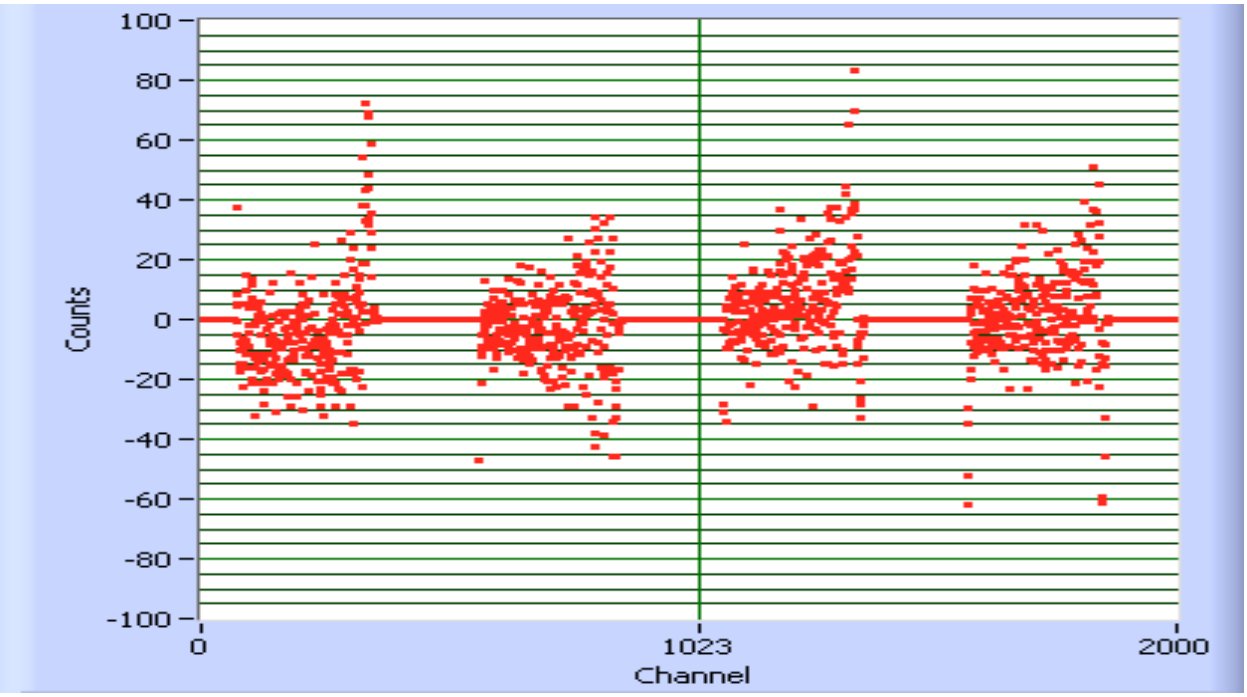

Figure 18: Residue of fit vs. measured data from Figure 16

In order to find the contribution of a dye to a mixture consisting of an equal volume of all 3 dyes in a sample, the equation is simply the count rate for the specific dye divided by the sum of the count rates for all the dyes. For example,

contribution 1 = count rate 1 / (count rate 1 + count rate 2 + count rate 3)

The same proportional method of analysis can be applied to the mixtures consisting of various quantities of each fluorophore. It can be assumed that the 10 µL of water in each run is negligible for the following reason. If water is present, it further dilutes the individual dyes equally in ratio. As only the ratios of the numbers of photons from each of the dyes are of interest, and these ratios are the same within the mixture with lesser concentrations, additional consideration is unnecessary. It can then be assumed that only the dyes are present in the mixture for this purpose. In this case, the contribution of a specific dye in a sample would be equal to its fraction of volume in the sample (without the water present) times its count rate. This is then divided by the total dyes in the sample, with respect to their individual fractions. An example to see the fractional contribution of Alexa 610 in a sample with 4µL of Alexa 610 and 16µL of Alexa 633 would be as follows:

*contrib. 610 = 4/20*count rate 610 / (4/20*count rate 610 + 16/20*count rate 633)*

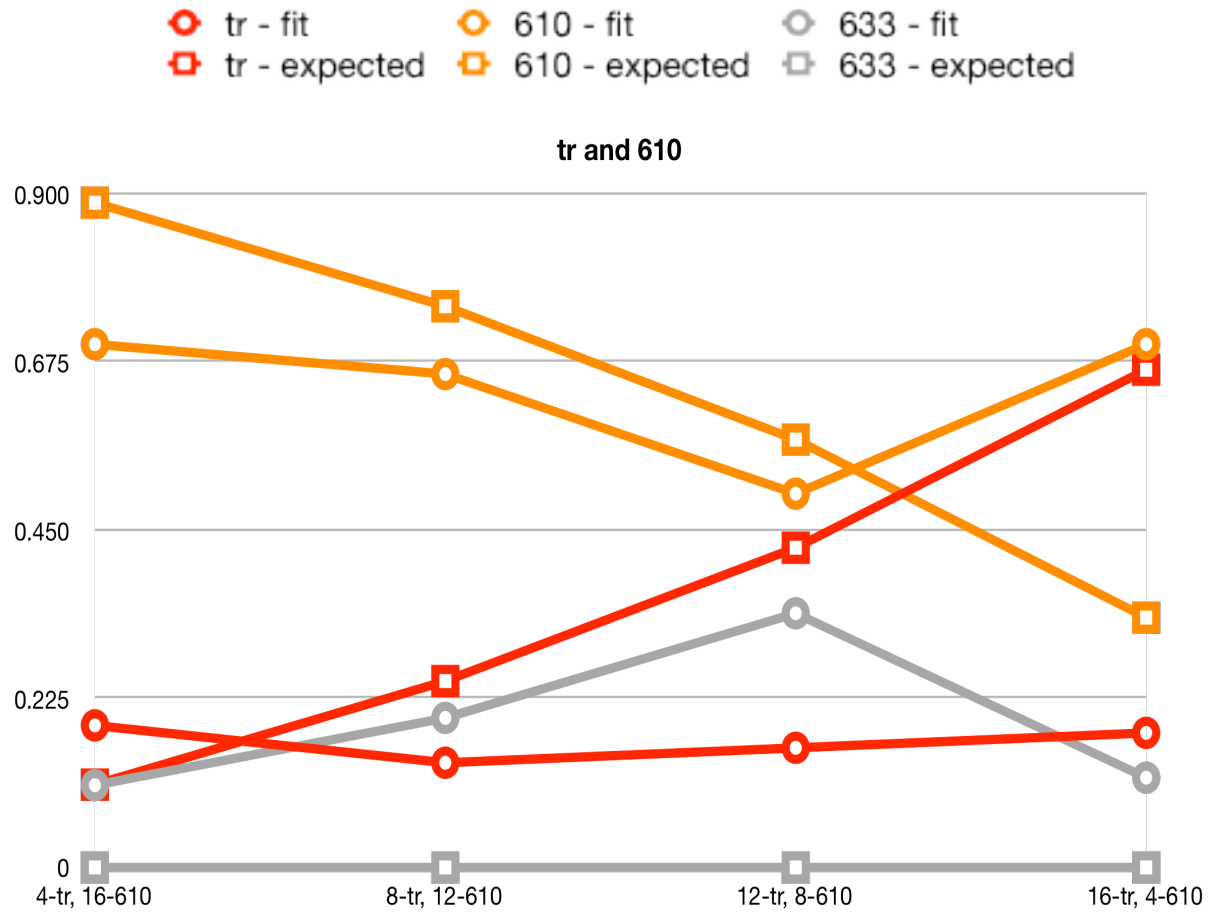

Figure 19: Calculated and fitted contributions for various quantities of Texas Red and Alexa 610 in a solution

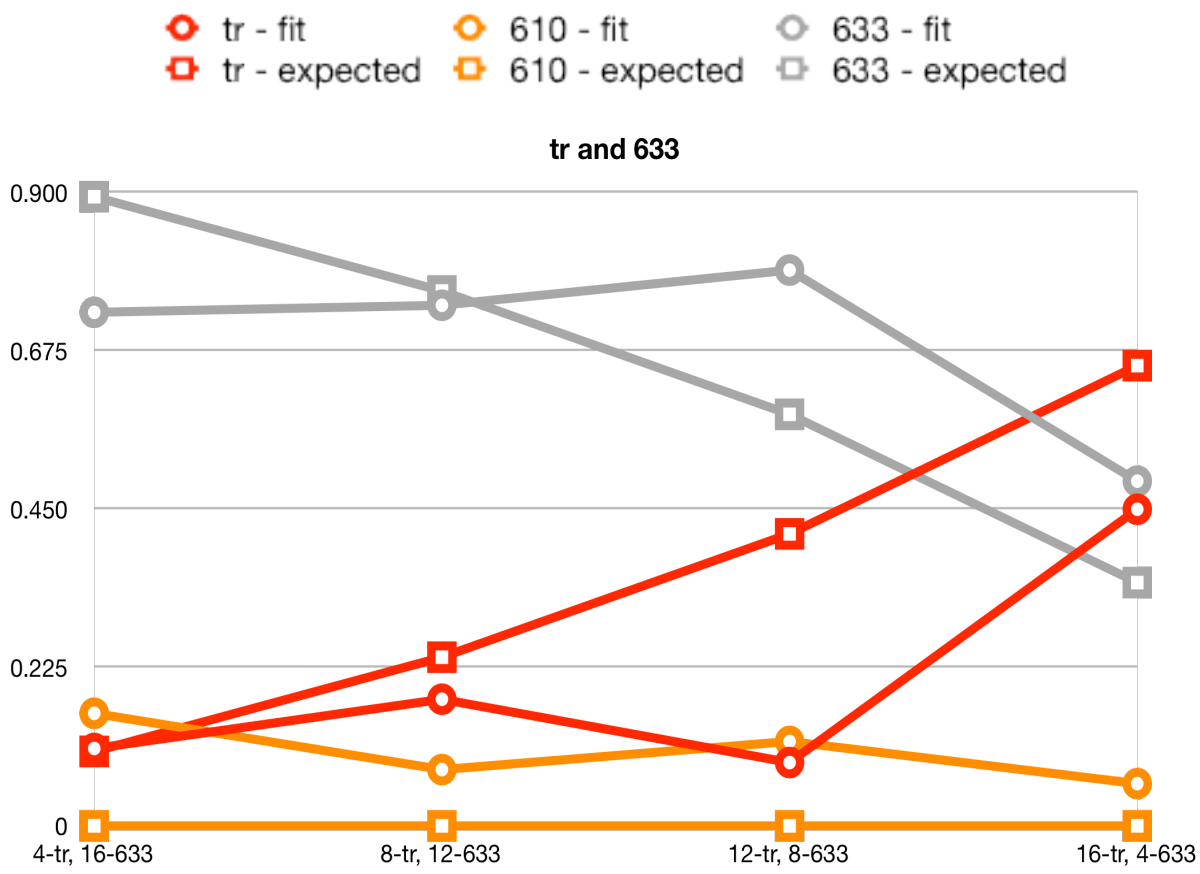

Figure 20: Calculated and fitted contributions for various quantities of Texas Red and Alexa 633 in a solution

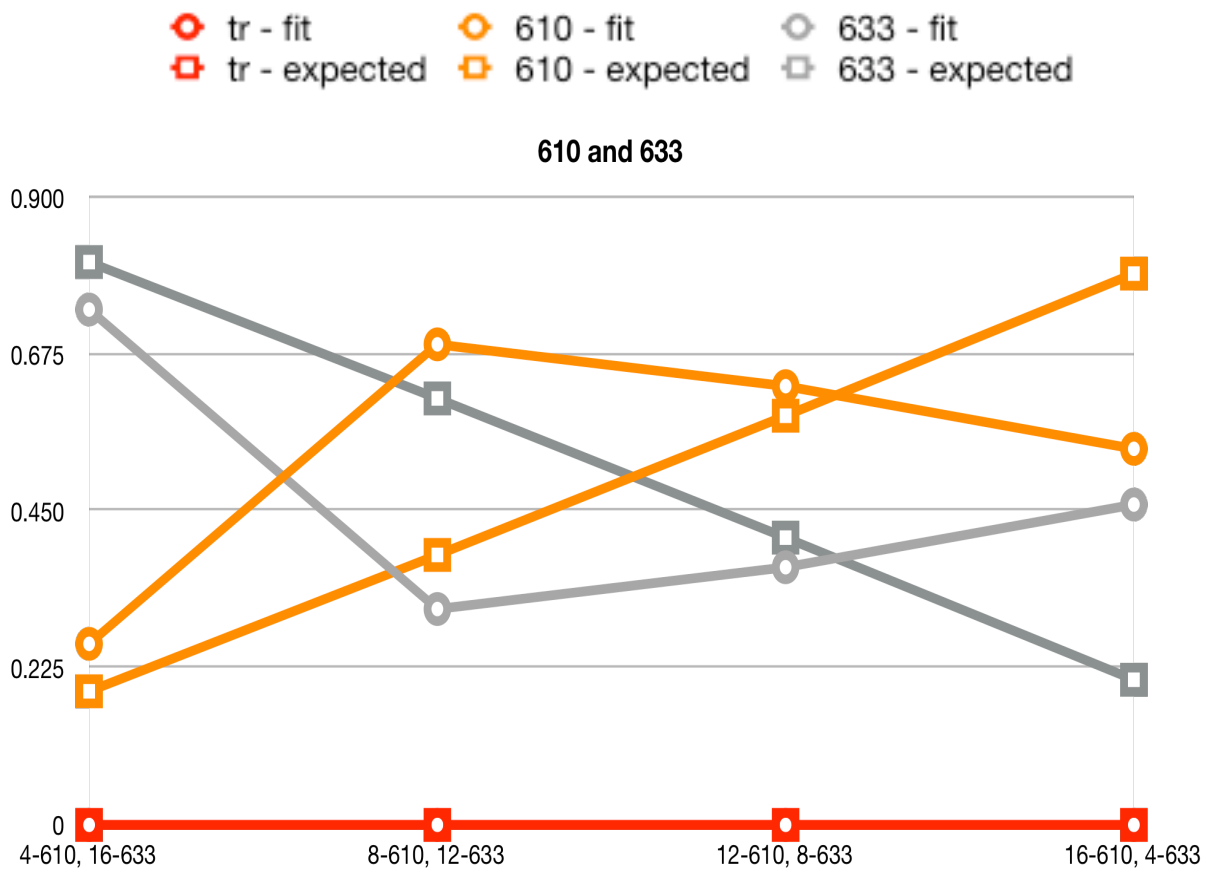

Figure 21: Calculated and fitted contributions for various quantities of Alexa 610 and Alexa 633 in a solution

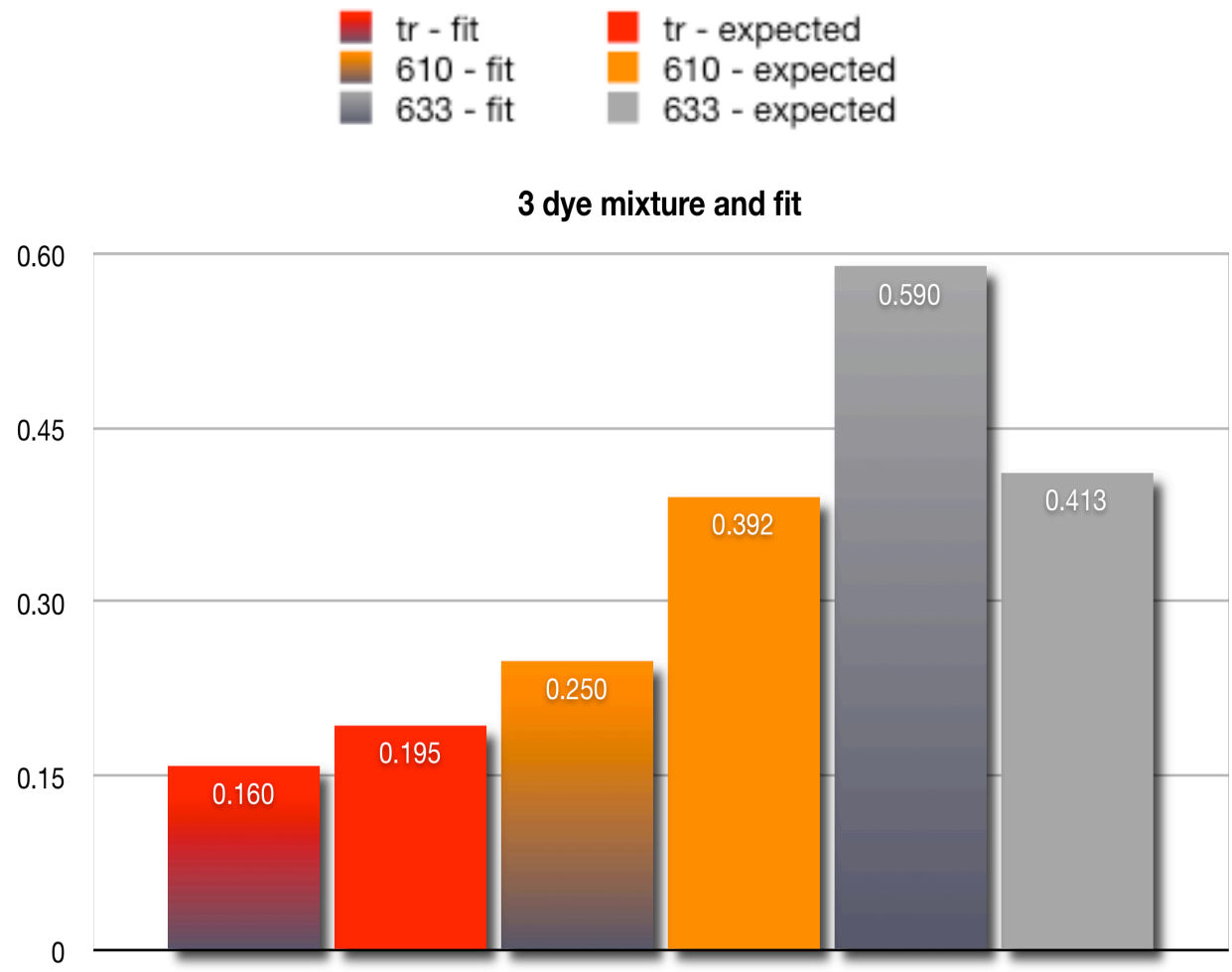

Figure 22: Equal volume contributions from each dye, showing calculated and fitted fractions of each in solution

Figure 17 clearly shows that the fit found by the ML algorithm is very close to that of the measured data. The fractional contributions found in Figures 19-22, however, indicate that for some of the mixtures it is not perfect with respect to accuracy. As the fit is almost identical to the measured data, one may conclude that the errors in the MLE analysis are random and possibly due to the level of shot noise present in the data.

Also, two distinct reasons for systematic errors come to mind. One involves an excess of shot noise. The MLE analysis assumes that the calibration curves are without noise. If there is any variance in the calibration curves, the MLE analysis is less likely to find accurate results. In this case, Poissonian shot noise could be enough to skew the pureness of the calibration curves. In order to alleviate this effect, collection times for the calibration runs should be increased to 3 or 5 minutes, to minimize the influence of shot noise.

Another possibility for systematic error is equipment malfunction. When doing these experiments, the dye laser was fluctuating in power, most probably caused by a change in humidity and temperature in the laboratory. These laser power fluctuations could cause inaccuracy in the calibration curves and, as above, lead to inaccurate MLE predictions.

Chapter VI

Conclusion

As each problem that occurred in this research brought a new knowledge, the final state came to be a solid and valid form. A confocal microscope for multiple wavelength time-resolved fluorescence detection with high throughput was built and a successful procedure was developed for unmixing the signal contributions of multiple fluorophores with overlapping spectral signatures. As expected, the precision of the unmixing becomes poorer for lower numbers of photons. Nevertheless, Figure 16 shows that the fit is accurate in comparison to the measured data. The number of counts per spectral band was in the range of 10^2— 10^3, which was the target requirement for a low photon count, as stated in the application for the grant to the National Institutes of Health, which provided partial support for this research. The results prove the usefulness of maximum-likelihood based unmixing for ultra-sensitive experiments.

The unmixing algorithm also proves useful when trying to conserve time for data analysis. Besides the general experimental set up, which accounts for approximately 5 minutes to create a slide, apply the wanted mixture, focus the laser into the sample, and record the data, the unmixing analysis is very quick. By simply loading the files into a Labview program and pressing Run, the process takes less than a second to analyze and unmix the species as well as graph out the findings and individual data curves. This

allows for many acquisitions to be taken and analyzed in a short period of time.

It is important to consider what can be done in the future to extend these methods. One of the first things that should be examined is how to apply rigorous error analysis. This will provide error bars for the fitted data, and thereby give insight as to how accurate the method performed. For the same purposes, studies using the Monte Carlo simulation should be extended to find the errors for particular combinations of dyes and the limits for unmixing in the ultrasensitive regime. However, simulation results should be compared to what is experimentally found.

Generalization of the method to other experimental configurations should be considered. One possibility is to bypass the use of an external counter and time-correlated single photon counting module and use the “smart” pixel 32x1 SPAD array developed by Tisa *et al.* [26]. They have created a detection head with internal electronics that time-tag single photons down to 3.2 μs. It combines ultra-sensitive detection (45% quantum efficiency) and high-speed acquisition (up to 312.5 kframe/s using a 10 MHz system clock). As the entire system is integrated, the pixel counts can be added from all channels to form one large SPAD, capable of viewing and entire spectra at once. This can prove useful as it cuts down optical components in the experimental layout. On the same lines, an EMCCD camera can provide fast frame rate acquisition for single-photon sensitivity experiments. The fluorescence can be focused onto a single line of pixels on

the camera, making it possible to take very fast frame rate measurements of the spectra by shifting the image to adjacent pixels as the new image is being acquired (the “fast kinetics” mode of data collection). A great advantage here is that the quantum efficiency is 95%, compared to the ~65% QE from the modified SPADs. The same maximum-likelihood data analysis method can be used, and the spectra can then be unmixed into the corresponding fractions of each species involved.

Another experimental option is to use two or more excitation wavelengths, as was done in reference [1]. A second excitation wavelength applied to the sample at ~630 nm will provide for another reference point in the data as the dyes are excited differently at each wavelength. This can further aid in distinguishing between the species as the emission peaks are more distinct than the emission tails.

Finally, an option to potentially add to the system is the phasor approach developed by Gratton’s group [27]. It builds up decays from vectors created by the image. Provided the modulation and phase of the emission with respect to the excitation can be found, the lifetime of each sample can be plotted onto a semicircular graph. As each dye has a unique lifetime, the possibility arises to use these as calibration plots for unmixing for a sample solution with multiple dyes present. This method could be coupled with the current ML method to possibly allow for greater accuracy, or to provide a check for consistency.

References

[1] Davis LM, Shen G. "*Extension of multidimensional microscopy to ultra-sensitive applications with maximum-likelihood analysis.*" Proceedings of SPIE Vol. 6443 (2007) 64430N 1-12

[2] Zimmermann, T. "*Spectral imaging and linear unmixing in light microscopy.*" Microscopy Techniques (Advances in Biochemical Engineering / Biotechnology) Ed. Jens Rietdorf. New York: Springer, 2005. 245-266

[3] Lippincott-Schwartz J, Patterson GH. "*Development and use of fluorescent protein markers in living cells.*" Science Vol. 300 Issue 5616 April 4, 2003: 87-91

[4] Lakowicz, JR. *Principles of Fluorescence Spectroscopy 2nd Edition*. New York: Springer, 2004

[5] Weisshart K, Jungel V, Briddon SJ. "*The LSM META ConfoCor 2 system: An integrated imaging and spectroscopic platform for single-molecule detection.*" Current Pharmaceutical Biotechnology Vol. 5 Issue 2 April 2004: 135-154

[6] Zucker RM, Price O. "*Evaluation of confocal microscopy system performance.*" Cytometry Vol. 44 Issue 4 August 1, 2001: 273-294

[7] Dinant C, van Royen ME, Vermeulen W, Houtsmuller AB. "*Fluorescence resonance energy transfer of GFP and YFP by spectral imaging and quantitative acceptor photobleaching.*" Journal of Microscopy-Oxford Vol. 231 Issue 1 July 2008: 97-104

[8] Dickinson ME, Simbuerger E, Zimmermann B, Waters CW, Fraser SE. "*Multiphoton excitation spectra in biological samples.*" Journal of Biomedical Optics Vol. 8 Issue 3 July 2003: 329-338

[9] Becker W, Bergmann A, Biskup C. "*Multispectral fluorescence lifetime imaging by TCSPC.*" Microscopy Research and Technique Vol. 70 Issue 5 May 2007: 403-409

[10] Li LQ, Davis LM. "*Single-photon avalanche-diode for single-molecule detection.*" Review of Scientific Instruments Vol. 64 Issue 6 June 1993: 1524-1529

[11] Cova S, Ghioni M, Lacaita A, Samori C, Zappa F. "*Avalanche photodiodes and quenching circuits for single-photon detection.*" Applied Optics Vol. 35 Issue 12 April 20, 1996: 1956-1976

[12] Giudice A, Biasi R, Rech I, Marangoni S, Labanca I, Simmerle G, Ghioni M, Cova S. "*Versatile electronic module for the operation of any silicon single photon avalanche diode.*" Journal of Modern Optics Vol. 56 Issue 2-3 2009: 317-325

[13] Stephens DJ, Allan VJ. "*Light microscopy techniques for live cell imaging.*" Science Vol. 300 Issue 5616 April 4, 2003: 82-86

[14] Wahl M, Koberling F, Patting M, Rahn H, Erdmann R. "*Time-resolved confocal fluorescence imaging and spectroscopy system with single molecule sensitivity and sub-micrometer resolution.*" Current Pharmaceutical Biotechnology Vol. 5 Issue 3 June 2004: 299-308

[15] Pelet S, Previte MJR, Kim D, Kim KH, Su TTJ, So PTC. "*Frequency domain lifetime and spectral imaging microscopy.*" Microscopy Research and Technique Vol. 69 Issue 11 November 2006: 861-874

[16] Ramadass R, Becker D, Jendrach M, Bereiter-Hahn J. "*Spectrally and spatially resolved fluorescence lifetime imaging in living cells: TRPV4-microfilament interactions.*" Archives of Biochemistry and Biophysics Vol. 463 Issue 1 July 1, 2007: 27-36

[17] Hanley QS, "*Spectrally resolved fluorescent lifetime imaging.*" Journal of the Royal Society Interface Vol. 6 Supplement 1 February 6, 2009: S83-S92

[18] Garini Y, Young IT, McNamara G. "*Spectral imaging: Principles and applications.*" Cytometry Part A Vol. 69A Issue 8 August 2006: 735-747

[19] Lansford R, Bearman G, Fraser SE. "*Resolution of multiple green fluorescent protein color variants and dyes using two-photon microscopy and imaging spectroscopy.*" Journal of Biomedical Optics Vol. 6 Issue 3 July 2001: 311-318

[20] Myung, IJ. "*Tutorial on maximum likelihood estimation.*" Journal of Mathematical Psychology Vol. 47 Issue 1 February 2003: 90-100

[21] Maus M, Cotlet M, Hofkens J, Gensch T, De Schryver FC, Schaffer J, Seidel CAM. "*An experimental comparison of the maximum likelihood estimation and nonlinear least squares fluorescence lifetime analysis of single molecules.*" Analytical Chemistry Vol. 73 Issue 9 May 1, 2001: 2078-2086

[22] King RL, Younan NH. "*Pixel unmixing via information of neighboring pixels.*" GIScience and Remote Sensing Vol. 43 Issue 4 October-December 2006: 310-322

[23] Enderlein J, Goodwin PM, VanOrden A, Ambrose WP, Erdmann R, Keller RA. "*A maximum likelihood estimator to distinguish single molecules by their fluorescence decays.*" Chemical Physics Letters Vol. 270 Issue 5-6 May 30, 1997: 464-470

[24] Hoppe AD, Shorte SL, Swanson JA, Heintzannz R. "*Three-dimensional FRET reconstruction microscopy for analysis of dynamic molecular interactions in live cells.*" Biophysical Journal Vol. 95 Issue 1 July 1, 2008: 400-418

[25] Chaplin M. "*Water absorption spectrum.*" Water Structure and Science 2009. London South Bank University. May 21, 2009. <http://www.lsbu.ac.uk/water/vibrat.html>

[26] Tisa S, Guerrieri F, Zappa F. "*SPAD detection head with 32 fully-parallel channels for time-tagging single-photons at 3 μs.*" Proceedings of SPIE Vol. 7222 (2009), 72221H 1-11

[27] Digman MA, Caiolfa VR, Zamai M, Gratton E. "*The phasor approach to fluorescence lifetime imaging analysis.*" Biophysical Journal Vol. 94 Issue 2 January 15, 2008: L14-L16

[28] "*Extension of multidimensional microscopy to ultra-sensitive applications with maximum-likelihood analysis*". 2009. University of Tennessee Space Institute. 22 July, 2009. <http://ldavis.utsi.edu/Max-likelihood%20unmixing.htm>

Vita

I was born in 1984 in York, Pennsylvania. I always knew I would end up doing something in math or music. It seems as if math won the battle for now. I finished my Bachelor of Science degree at James Madison University in the major or Physics. And now I am at the University of Tennessee Space Institute, writing a thesis on spectral fluorescence lifetime imaging. All throughout high school and college, I've been in and out of the hospital, getting surgery on my brain and spine. Yet it has never stopped me from achieving what I have and never stopped me from becoming the person I wanted to be. For that, I take pride in my achievements and for getting to where I am this day. I can only hope that I continue to prosper as the future unfolds.